European Journal of Medicinal Chemistry 276 (2024) 116647

Contents lists available at ScienceDirect

European Journal of Medicinal Chemistry

journal homepage: www.elsevier.com/locate/ejmech

Research paper

Discovery of pyridoquinoxaline-based new P-gp inhibitors as coadjutant against Multi Drug Resistance in cancer

Roberta Ibba [a,1], Simona Sestito [b,1], Francesca Alessandra Ambrosio [c], Emanuela Marchese [c], Giosuè Costa [c,d], Francesco Paolo Fiorentino [e], Fabio Fusi [f], Irene Marchesi [e], Beatrice Polini [g], Grazia Chiellini [g], Stefano Alcaro [c,d], Sandra Piras [a,*], Antonio Carta [a]

[a] Department of Medicine, Surgery and Pharmacy, University of Sassari, 07100, Sassari, Italy
[b] Department of Chemical, Physical, Mathematical and Natural Sciences, University of Sassari, 07100, Sassari, Italy
[c] Department of Health Sciences, University "Magna Græcia" of Catanzaro, Campus "S. Venuta", 88100, Catanzaro, Italy
[d] Net4Science Academic Spin-Off, University "Magna Græcia" of Catanzaro, Campus "S. Venuta", 88100, Catanzaro, Italy
[e] Kitos Biotech Srls, Tramariglio, Alghero, SS, Italy
[f] Department of Biotechnologies, Chemistry and Pharmacy, University of Siena, 53100, Siena, Italy
[g] Department of Pathology, University of Pisa, 56100, Pisa, Italy

ARTICLE INFO

Keywords:
Multi-drug resistance
Cancer
P-glycoprotein
Quinoxaline derivatives
ADME prediction
Docking studies

ABSTRACT

Multi-drug resistance (MDR) is a serious challenge in contemporary clinical practice and is mostly responsible for the failure of cancer medication therapies. Several experimental evidence links MDR to the overexpression of the drug efflux transporter P-gp, therefore, the discovery of novel P-glycoprotein inhibitors is required to treat or prevent MDR and to improve the absorption of chemotherapy drugs via the gastrointestinal system. In this work, we explored a series of novel pyridoquinoxaline-based derivatives designed from parental compounds, previously proved active in enhancing anticancer drugs in MDR nasopharyngeal carcinoma (KB). Among them, derivative **10d** showed the most potent and selective inhibition of fluorescent dye efflux, if compared to reference compounds (MK-571, Novobiocin, Verapamil), and the highest MDR reversal activity when co-administered with the chemotherapeutic agents Vincristine and Etoposide, at non-cytotoxic concentrations. Molecular modelling predicted the two compound **10d** binding mode in a ratio of 2:1 with the target protein. No cytotoxicity was observed in healthy microglia cells and off-target investigations showed the absence of $Ca_V1.2$ channel blockade. In summary, our findings indicated that **10d** could potentially be a novel therapeutic coadjutant by inhibiting P-gp transport function *in vitro*, thereby reversing cancer multidrug resistance.

1. Introduction

Multi-drug resistance (MDR) is one of the leading causes of cancer treatment failure and a major challenge in modern clinical practice. Either intrinsic at the stage of diagnosis or acquired throughout treatment, MDR results in the concomitant resistance of the cancer patient to multiple chemotherapeutic agents. MDR occurs in cancer through various mechanisms, such as downregulation of cell death signals, drug sequestration in intracellular compartments, microenvironmental adaptation, and increased expression of drug efflux transporters, limiting or abrogating the effectiveness of a single or combined anticancer treatment [1].

ATP-binding cassette (ABC) is one of the widest families of transmembrane transporters, found in human, animal and plant cells [2]. Human cells express forty-eight members from seven different families (ABCA-ABCG). Nearly twenty of them act as drug efflux pumps, including ABCB1, widely known as *MDR1 multidrug resistance protein 1* or *Permeability glycoprotein* (P-gp), ABCC1/MRP1 - *MDR-associated protein 1*, and ABCG2 or BCRP - *breast cancer resistance protein*. These isoforms are universally expressed across MDR cancer cells and share a

* Corresponding author.
E-mail addresses: ribba@uniss.it (R. Ibba), ssestito@uniss.it (S. Sestito), ambrosio@unicz.it (F.A. Ambrosio), e.marchese@unicz.it (E. Marchese), gcosta@unicz.it (G. Costa), fpfiorentino@kitosbiotech.org (F.P. Fiorentino), fabio.fusi@unisi.it (F. Fusi), imarchesi@kitosbiotech.org (I. Marchesi), beatrice.polini@farm.unipi.it (B. Polini), grazia.chiellini@unipi.it (G. Chiellini), alcaro@unicz.it (S. Alcaro), piras@uniss.it (S. Piras), acarta@uniss.it (A. Carta).
[1] These authors contributed equally.

https://doi.org/10.1016/j.ejmech.2024.116647
Received 5 April 2024; Received in revised form 30 June 2024; Accepted 1 July 2024
Available online 7 July 2024

common ability to extrude substrates, including chemotherapy agents, from the cytoplasm to the extracellular environment, thus reducing their intracellular accumulation [3–5].

P-gp is a 170 kD transmembrane glycoprotein consisting of two transmembrane domains (TMD) and two nucleotide-binding domains (NBD). Looking at its native activity, P-gp recognizes a wide range of xenobiotics/chemotherapeutics with no prerequisite for structure similarity and actively transports them outside the plasma membrane consuming two ATP molecules. Being widely expressed in different tissues and blood–organ barriers, in physiological conditions P-gp plays a protecting role, preserving cells and tissues from toxic substances. P-gp represents a major factor for pleiotropic MDR in clinical contexts, as reported in several studies that observed P-gp was highly expressed or overactivated in many patients resistant to chemotherapy [6]. Moreover, intestinal P-gp extrudes chemotherapeutics in the intestinal lumen, limiting oral absorption and bioavailability [7].

Lately, P-gp has regained its importance for being reported as a main cause for intrinsic and acquired resistance to new therapeutic approaches, such as targeted agents. Up-regulation of P-gp related to treatment resistance has been reported for kinase inhibitors [8] and, more recently, PROTACs' activity was proved affected by P-gp overexpression [9]. Intriguingly, Kurimchak and colleagues ascertained that early co-administration of P-gp inhibitors and PROTACs inhibits the efflux pump overexpression, preventing the development of drug resistance [9]. Therefore, an effective P-gp inhibitor could not only reverse MDR, or avoid it by early co-administration, but also potentiate the absorption and the efficacy of standard chemotherapeutics, allowing the reduction of the administered dose and the related side effects [7].

Inspired by the potential of this multifaceted pharmacological tool, medicinal chemists developed different generations of P-gp inhibitors over the last decades. First-generation include quinidine, cyclosporine A, and verapamil, which were rapidly set aside due to low therapeutic efficacy, limited selectivity, and drug toxicity [10–14]. Some improvements in activity and selectivity were achieved with the second generation (Valspodar, Dexverapamil, S9788 and Biricodar), but the clinical application was limited by high toxicity and the concerted inhibition of CYP3A4, responsible for the consequent undesirable drug-drug interactions [15–17]. Third-generation inhibitors, such as Elacridar, Tariquidar, Zosuquidar and Laniquidar possessed higher affinities and selectivity to P-gp and lower CYP3A4 inhibition compared with the previous generation of P-gp inhibitors, but they failed clinical phase due to interference with MRP1/ABCC1 and adverse toxicity in combination with chemotherapeutic agents [18,19]. Although challenging, the development of new P-gp inhibitors has never stopped, and many inhibitors have also been identified by repurposing FDA-approved drugs [20].

Like other ABC transporter family members, P-gp contains two binding areas, the ATP-binding site, and the drug binding site, both investigated for drug development. Most of the currently developed P-gp inhibitors behave as competitive inhibitors of the drug-binding site, located in TMD, or as non-competitive inhibitors targeting the ATP binding site in NBD [21,22]. Despite ABC proteins being able to transport a wide range of substrates with a high structural allowance and functionally unrelated, many novel candidates share common features such as several favorable physio-chemical properties (i.e., the presence of aromatic portion, certain lipophilicity, and a positive charge at neutral pH) and some preferential scaffolds. For instance, most of the third-generation inhibitors bear a tetrahydroisoquinoline moiety, while recent candidates present different bicyclic N-heterocycles cores such as quinoline [23], triazole-pyrimidine [24], and quinoxaline [25,26], among others.

In this context, we previously synthetized a series of 6-trifluoromethyl-quinoxalines which were capable of restoring or potentiating the antiproliferative activity of Doxorubicin, Vincristine and Etoposide in MDR nasopharyngeal carcinoma KB cell lines [27,28]. The obtained results have driven us to design a new series of P-gp inhibitors by expanding the quinoxaline core with a pyridine cycle (blue in Fig. 1) in place of trifluoromethyl moiety and studying the impact of different side chains (orange in Fig. 1) on the P-gp inhibition activity. The heterocyclic core-expansion approach was selected to improve lipophilicity and steric hindrance and to gain an increased occupancy of the binding site. The pyridoquinoxaline compounds synthetized bear a couple of equal side chains in positions 2 and 3 of the pyridoquinoxaline ring [29]. Then, we explored more in depth the influence of different side chains in the occupancy of the P-gp channel. Therefore, in this work, we described the development of a new series of 2,3- variably substituted pyridoquinoxaline-based derivatives as potential P-gp inhibitors and we explored their ability to reverse MDR in cancer cell lines, combining them with standard anticancer drugs in different cancer subtypes.

2. Results

2.1. Chemistry

The final synthetic route (Scheme 1) was designed through a retrosynthetic approach, then it was set and optimized to gain the desired pyridoquinoxaline final compounds. The synthesis of the key intermediated **7** was previously described [30] and here improved. The building of the main pyridoquinoxaline scaffold **8**, properly halogenated, allowed the last alkylation step carried out by adding two equivalents of chains **9a-i** (Fig. S1) to get the desired final compounds **10a-i**. Compound **13d** is the sole benzoquinoxaline derivative of the series, designed and synthetized to evaluate the role of the pyrido nitrogen in the target binding.

To investigate the different occupancy levels of the wide channel within the target, differently functionalized chains **9a-i** (Fig. S1) were designed and synthetized to increase the number of heteroatoms and the steric hindrance. The smaller chains 4-cyanophenol **9a**, methyl vanillate **9b** and methyl thiosalicylate **9c** were commercially purchased. Whereas 2-phenol-carboxamide compounds **9d-i** were properly synthetized as shown in Scheme 2 by activation of salicylic acid (**14**) or 5-chloro salicylic acid (**15**), followed by amide formation with the appropriate anilines **16d-i**.

2.2. Biological evaluation

2.2.1. Cell line selection

As a first step of the study, we needed to identify suitable models to evaluate the potential activity of our pyridoquinoxaline compounds. Aiming to explore the eventual interaction with the whole ABC family, we assessed gene expression of the specific isoform ABCB1, -C1, -G1 and -G2 in various cancer cell lines in the publicly available dataset (Fig. 2A) [31]. Among them, we selected four human cancer cell lines: A498 (renal carcinoma), CAKI2 (renal carcinoma), HCT15 (colorectal carcinoma) and HT1197 (bladder carcinoma) for their different ABC isoform expression (Fig. 2B). While A498 presents a wide spectrum of transporters at different levels of expression, the other cell lines show higher expression of one of the four ABC members and were therefore chosen as representative models: CAKI2, HCT15, and HT1197 for -C2, -B1 and -G2, respectively.

2.2.2. Drug efflux inhibition

Effects on MDR efflux pumps were assessed in cultured cells using EFLUXX-ID Green multidrug resistance assay kit (ENZO Life Sciences, Cat. No. ENZ-51029-K100) in the presence or absence of potential ABC inhibitors. The reagent provided within the kit is a hydrophobic non-fluorescent compound that penetrates the cell membrane and is subsequently hydrolysed inside the cells by intracellular esterases, gaining the chemical probe, a hydrophilic green-fluorescent dye that is trapped within the cell unless actively pumped out by an active ABC transporter. The fluorescence signal of the dye generated within the cells thus depends upon the activity of the ABC transporters. Being a substrate for

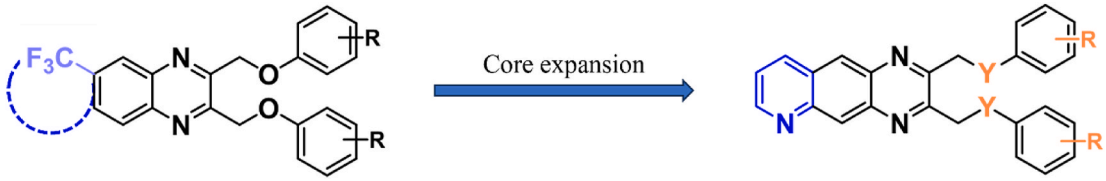

Fig. 1. Rational design of new pyridoquinoxaline-based derivatives as potential P-gp inhibitors.

ABCB1, ABCC1/2 and ABCG2, the reagent is an indicator of these proteins' activity in the cell. The cells with highly active transporters demonstrate lower fluorescence because of the active efflux of the dye from the cell. Therefore, we examined the effect on green-fluorescence induced by compounds **10a-i** and **13** at three different concentrations (0.1, 1 and 10 μM) in the selected cell lines. Three well-known ABC transporter inhibitors were used as positive control at their active concentration, as single agents or in combination: Verapamil (20 μM), MK-571 (50 μM), and Novobiocin (200 μM), inhibitors for ABC-B1, ABC-C1/2 and ABC-G2, respectively. Panels in Fig. 3 showed that all the tested compounds led to a certain dye accumulation in all the cell lines except for A498, which turned out to be the most resistant one. Conversely, HCT-15 cells were the most susceptible to the administration of our compounds and allowed the outline of structure-activity relationships (SARs). We found that increasing the number of phenyl rings (from **10a-c** to **10d-h**) did not deeply impact the activity; analogously, inserting a methoxyl-substitution on the additional phenyl ring (**10d** vs **10e**) the efficacy was not improved, while the dose-response profile was inconsistent, favoring the parental **10d**. The addition of a chlorine atom to the phenolic moiety, on the contrary, significantly decreased the retention of the green fluorescent probe. Also, the inhibition activity was greatly reduced when the steric hindrance of chlorine derivatives was increased by raising the number of methoxy groups from one (**10f**) to two and three (**10g** and **10h**). We also observed a significant reduction in the transporter's inhibition when comparing compound **13d**, designed to assess the relevance of the nitrogen atom on the pyridine ring, to compound **10d** which gains the mentioned nitrogen atom. Among all the tested derivatives, compound **10d** was selected for further investigation for its activity and selectivity. We sporadically detected a decreased activity at the highest concentration (10 μM) most certainly due to insolubility of compounds in assay conditions. Derivative **10d** exerted a significant activity in HCT-15 cells, higher-expressing ABCB1, and poorly inhibited efflux in CAKI2 cells, while turned out completely inactive in HT1197 and A498 cell lines. Data analysis in HCT-15 suggests a dose-dependent activity with a remarkable increase in fluorescence at 0.1 and 1 μM, while a less significant activity was identified growing **10d** concentration from 1 to 10 μM. Notably, **10d** resulted in comparably active and more selective than the reference drug Verapamil, which exerted moderate activity in all the tested cellular models. A direct comparison of the two ABC inhibitors is not definable as they have been tested at different concentrations. However, it can be observed that compound **10d** at 10 μM doubled the green fluorescence intensity while Verapamil at 20 μM concentration turned out slightly more efficacious.

Due to its selectivity and potency, **10d** was selected to deeply investigate its pharmacological profile.

2.2.3. Concentration selection and association with standard chemotherapy

To evaluate the potential MDR reversal activity, cell proliferation assays were performed by treating selected cell lines with hit compound **10d** in combination with Vincristine or Etoposide. The co-administered drugs were selected among the anticancer agents most used in therapeutic protocols, but they also represent widely recognized ABC-B1 clients [32–35].

Compound **10d** was initially tested at variable concentrations (0.25, 0.5, 1, and 4 μM) together with a fixed dose of vincristine (0.2 μM), in several cancer cell lines such as A498, A704 (renal adenocarcinoma) and U87-MG (glioma). We observed an evident upsurge in vincristine potency when co-administered with compound **10d** at all the tested concentrations (Fig. 4A). Subsequently, to deepen co-administration investigation, we treated a larger panel of cell lines with a fixed concentration of **10d** (4 μM) and a scaling dosage of Vincristine ranging from 0.02 up to 20 μM. Representative eight cell lines of human cancer types characterized by different Vincristine responsiveness were selected. The first four cell lines shown in Fig. 4B, SK-HEP-1 (hepatic adenocarcinoma), HGC-27 (human gastric carcinoma), HupT3 (human pancreatic adenocarcinoma), Mewo (human melanoma) turned out sensitive to the drug treatment and less responsive to the co-administration with the MDR-reversal compound **10d** (Fig. 4B). In the same experiment, HT-29 (colorectal adenocarcinoma), U-87-MG, A498 and A704 cell lines showed drug resistance to Vincristine in monotherapy, and the co-administration with our P-gp inhibitor restored drug efficacy. As depicted in Fig. 4B, compound **10d** triggered the cytotoxic activity of Vincristine both in sensitive cell lines (HGC-27 and HupT3) and resistant cancer cells, cutting the percentage of cell growth by half, as found in treated A498 and A-704 cancer cell lines.

The same cell lines were also treated with the sole **10d** at 4 μM concentration to assess if the increased cytotoxic effect obtained by the co-administration of **10d** and vincristine was ascribable to the inhibition of the drug efflux and not caused by a potential additive activity. As shown in Fig. 5, **10d** has a very low/low potential for toxicity at 4 μM except for HGC27 and A498, were **10d** triggered a reduction in percentage of growth ranging from around 40 and 20 %, respectively.

Analogously, **10d** 4 μM was tested in selected cell lines (A498, A704, U87-MG, and SK-N-SH) in association with Etoposide at 40, 4, 0.4 and 0.04 μM concentrations. Results depicted in Fig. 6 show that cell growth is consistently decreased when etoposide is co-administered with **10d** inhibitor compared to single etoposide treatment, resulting in improved drug efficacy. The sole exception concerns SK-N-SH where the co-administration with our MDR reversing agent is slightly relevant in the cytotoxic effect observed in this cell line, being already highly sensitive to the treatment with Etoposide.

2.2.4. Association with cisplatin

To further confirm **10d** MDR reversal activity, an analogue assay was performed as negative control by using a non-transported anticancer drug, such as cisplatin [36]. The drug was administered alone or in combination with compound **10d** in HT-29, HupT3, SK-HEP1 and HCT116 as representative of cisplatin-sensible cancer types. The co-treatments were performed in different combinations, firstly by administering a fixed dose of compound **10d** (1 μM) and variable doses of cisplatin, from 0.1 up to 100 μM (Fig. 7A); results showed a detectable resistance of cells to treatment. Then cisplatin was administered at the fixed concentration of 0.25 μM (not saturating and poorly active dose) and a scaling dose of P-gp inhibitor, from 0.25 up to 4 μM, (Fig. 7B). As expected, the combination of cisplatin with our P-gp inhibitor did not produce a significant increase in cisplatin cytotoxic effect.

2.2.5. Cytotoxicity

In order to complete the cellular studies, we would assess if **10d** may exert cytotoxicity in healthy cells. Thus, we treated the human microglial clone 3 cell line (HMC3), used as sensitive non-cancerous cells, with increasing doses (0.1–100 μM) of **10d** and cytotoxicity was measured at

Synthesis of key intermediates

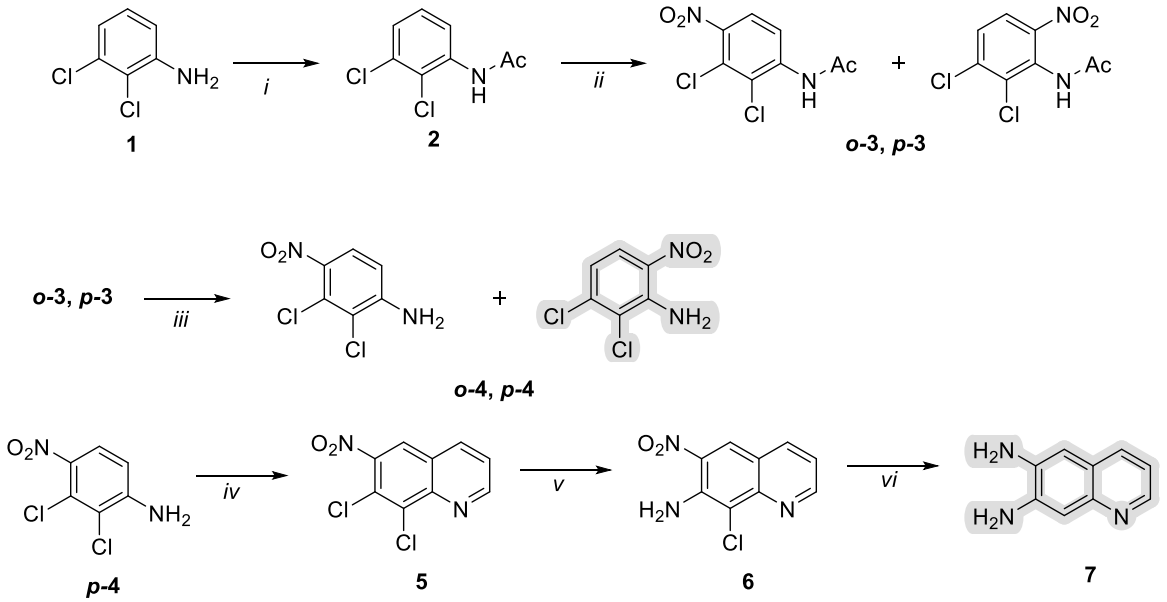

Synthesis of key quinoxaline-based final compounds

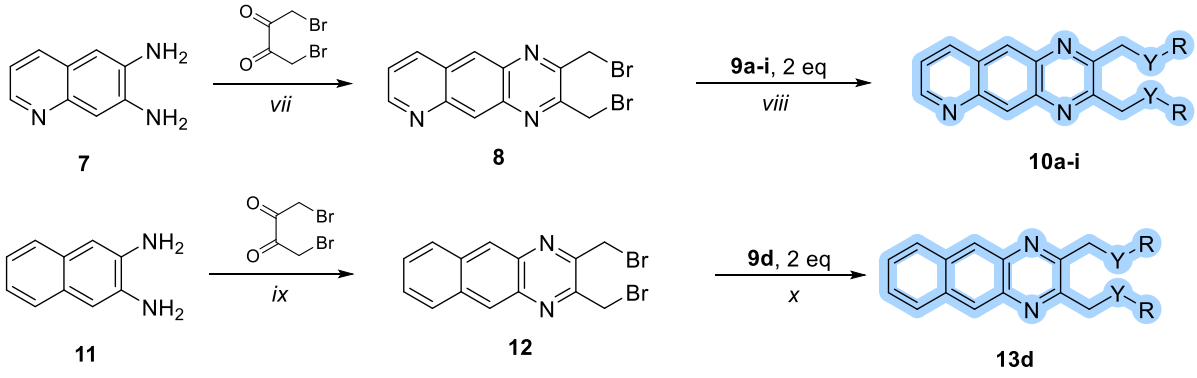

	Y	R
a	O	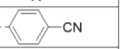
b	O	
c	S	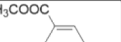
d	O	
e	O	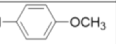
f	O	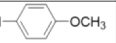

	Y	R
g	O	
h	O	
i	O	

Scheme 1. Synthetic route to obtain tricyclic derivatives **10a-i** and **13d**. Key intermediates are highlighted in grey, general structure of final compounds are highlighted in pale blue. *i.* acetic anhydride, r.t., 2h; *ii.* KNO_3/H_2SO_{4conc}, 0 °C to r.t., 24h; *iii.* H_2SO_{4conc}, 100 °C, 2h; *iv*. Skraup synthesis with glycerol, $As_2O_5 \cdot H_2O$, H_2SO_{4conc}, 150 °C, 2h; *v*. $NH_3/EtOH_{ss}$, 100 °C, autoclave, 24h; *vi*. $NH_2NH_2 \cdot H_2O$, Pd/C, EtOH, 80 °C, 2h. *vii.* 1,4-dibromobutane-2,3-dione, EtOH, 80 °C, 15 min; *viii*. NaOH, BTAC, $CHCl_3/H_2O$, 60 °C; *ix*. 1,4-dibromobutane-2,3-dione, EtOH, 80 °C, 15 min; *x*. NaOH, BTAC, $CHCl_3/H_2O$, 60 °C.

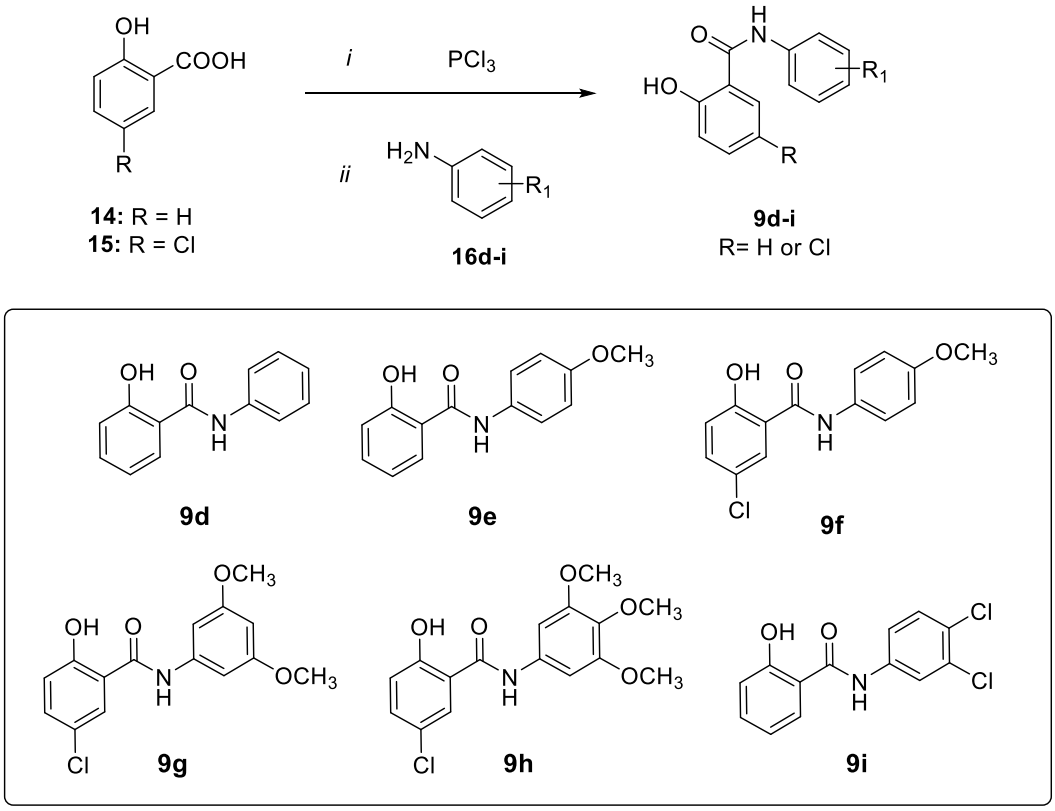

Scheme 2. Synthetic route carried out to gain intermediate chains **9d-i**, . Synthetic route carried out to gain intermediate chains **9d-i**, general structure highlighted in light purple, single intermediate structures are reported in the box. *i.* Chlorobenzene, reflux; *ii.* chlorobenzene, reflux.

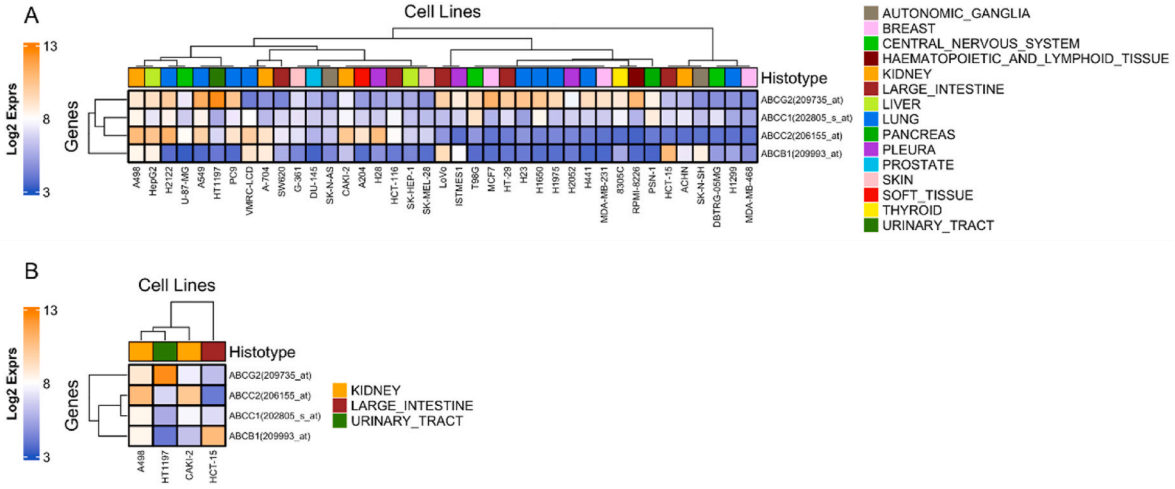

Fig. 2. Gene expression for ABC members ABC-B1, -C1, -C2 and -G2 in publicly available dataset (cancer cell line encyclopedia). The graph reports the cell lines on the x-axis, the 4 genes are reported on the y-axes; the histotypes are identified by colors and the legend is on the right of the figure. Gene expression is described as fold change reported as Log2 expression; values from 3 as physiological expression to 13 as maximum rate of over-expression, are used.

different time points (24, 48, and 72 h). Results graphed in Fig. 8 revealed that **10d** does not elicit any significant toxicity in this non-cancer cell line at all concentrations tested per each time point analyzed. Vehicle-treated cells have been used as control.

2.3. Molecular modeling studies

Considering the ability of the known P-gp inhibitor Encequidar to occupy both the drug-binding site and the access tunnel of the target protein [37], the aim of our modeling analysis was the investigation of compound **10d** capability to bind the same sites.

Notable, molecular recognition results revealed that **10d** is able to recognize both the P-gp active site and the access tunnel (Fig. 9A) with a good theoretical binding affinity (Table 2).

The ligand is well accommodated in the investigated P-gp sites, establishing different kinds of interactions with the key residues of both the binding pocket and the access tunnel (Fig. 9B).

In detail, compound **10d** is engaged in two π-stacking interactions with Tyr950 and Phe983 (bond lengths 4.64 Å and 4.19 Å), in a hydrogen bond with the Glu875 (bond length 2.12 Å), and three

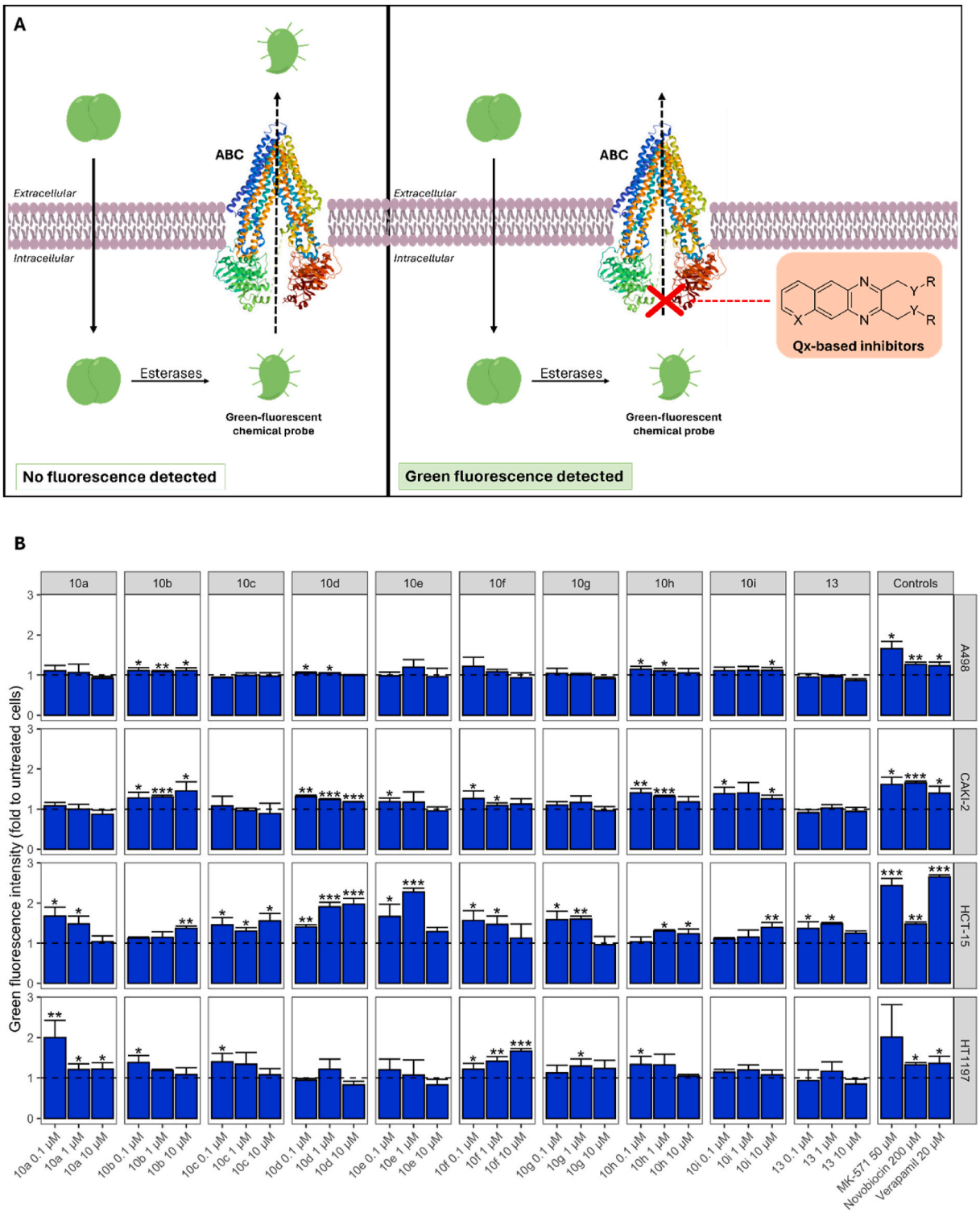

Fig. 3. A) Graphical representation of the drug efflux inhibition assay. **B)** ABC transporter's green-fluorescent substrate accumulation in A498, CAKI-2, HCT-15, and HT1197 cell lines treated with potential ABC inhibitors and positive control, relative to untreated cells. Values are shown as mean ± SD. *$p < 0.05$, **$p < 0.01$, or ***$p < 0.001$.

aromatic H-bond interactions, respectively, with Glu875, Ser979 and Gln990 (bond lengths 3.26 Å, 3.49 Å and 3.47 Å). In addition, the ligand is stabilized by several hydrophobic contacts with Leu65, Met68, Met69, Gln195, Thr199, Phe336, Ser344, Phe732, Ala871, Gly872, Glu 875, Gln946, Met 949, Tyr950, Tyr953, Ser979, Phe983, Met986, and Gln990.

Considering the access tunnel, we found that compound **10d** establishes two π-stacking interactions with Tyr307 and Phe728 (bond lengths 4.03 Å and 4.42 Å), respectively. Moreover, the ligand is engaged in a hydrogen bond with the Trp232 (bond length 2.01 Å) and two aromatic H-bond with Asn721 (bond lengths 3.02 Å and 3.27 Å). In addition, several hydrophobic contacts with Trp232, Ile299, Phe303, Tyr307, Tyr310, Ile340, Phe343, Ser344, Asn721, Leu724, Phe728, Gln938, Ala987, Gln990, Val991, and Phe994 are established.

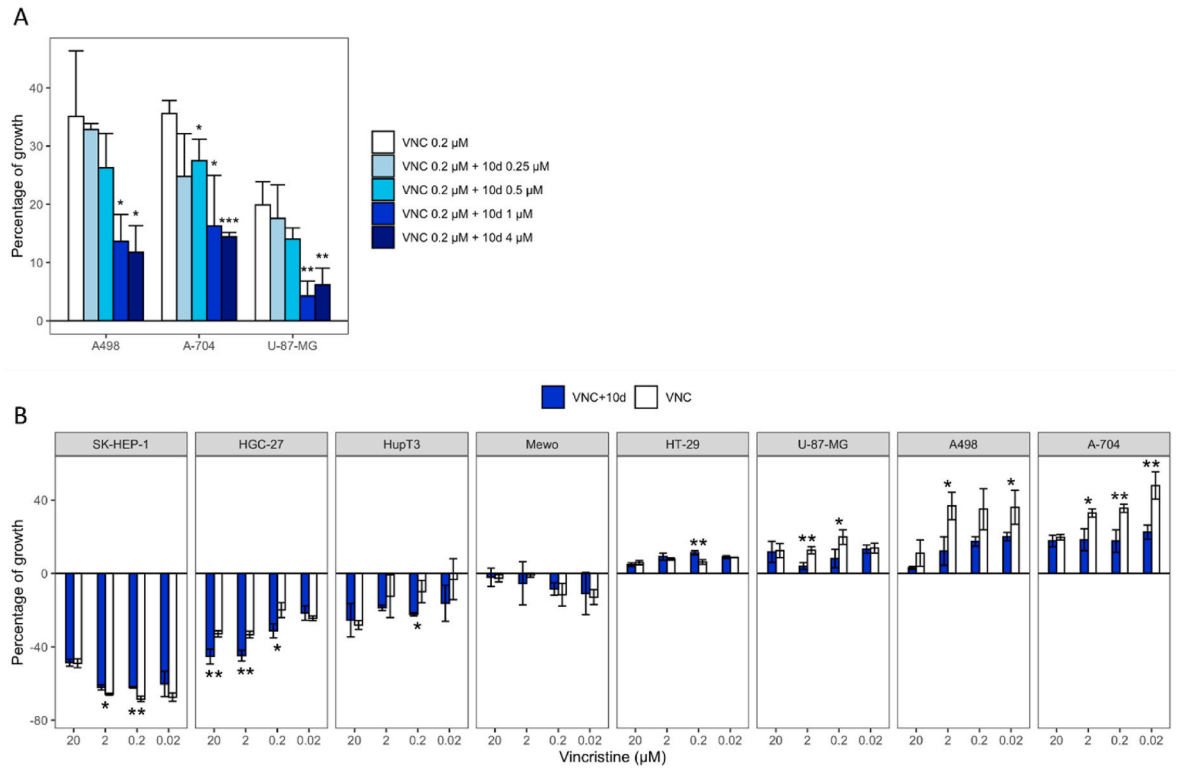

Fig. 4. **A)** Growth inhibition activity of vincristine (0.2 μM) alone or co-administered with different doses of **10d** (0.25, 0.5, 1 and 4 μM) in A498, A704 and U87-MG cell lines. **B)** Growth inhibition activity of vincristine at four different concentrations (20, 2, 0.2 and 0.02 μM) in mono treatment or associated to **10d** (4 μM) in SK-HEP-1, HGC-27, HupT3, Mewo, HT29, U87-MG, A498 and A-704 cell lines. Values are shown as mean ± SD. *p < 0.05, **p < 0.01, or ***p < 0.001 and are normalized to DMSO treatment. A percentage of growth between 0 and 100 indicates reduced cell growth, while a value between 0 and -100 indicates cell death.

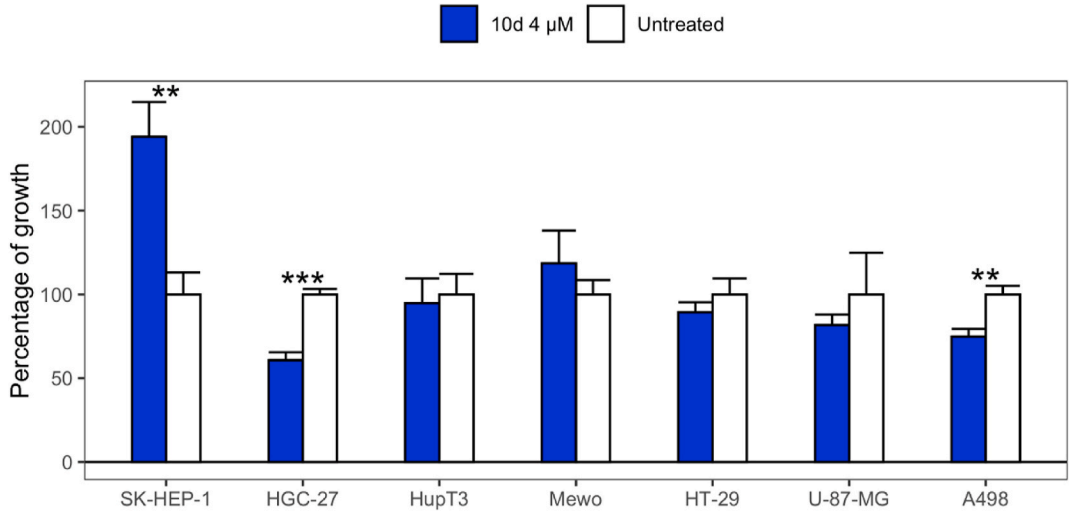

Fig. 5. Growth inhibition effect of **10d** (4 μM) in different cancer cell lines (SK-HEP-1, HGC-27, HupT3, Mewo, HT29, U87-MG and A498). Values are shown as mean ± SD. *p < 0.05, **p < 0.01, or ***p < 0.001.

Noteworthy, the two **10d** molecules interact with each other establishing a π-stacking interaction and different hydrophobic contacts between their terminal phenyl moieties (Fig. 9C).

2.4. Off-target evaluation: Cav1.2 channel blockade

Off-targets represent a major issue in drug development and early toxicity evaluation could prevent clinical trial attrition. The Cav1.2 channel blocker Verapamil belongs to the first generation of P-gp inhibitor; despite the efforts to reduce cardiovascular effects by enhancing the P-gp activity, the second generation dexverapamil still presents a residual cardiac side effect, and, generally, interference with Cav1.2 channels may lead to cardiotoxicity and limited clinical success. Therefore, we investigated the potential interaction of **10d** with the Ba^{2+} current through $Ca_V1.2$ channels ($I_{Ba1.2}$). As reported in Fig. 10, the addition of cumulative concentrations (0.3–10 μM) of **10d** did not affect peak $I_{Ba1.2}$ elicited with a clamp pulse to 10 mV from a V_h of −50 mV (0.067 Hz), implying a potential non-cardiotoxic effect for this compound.

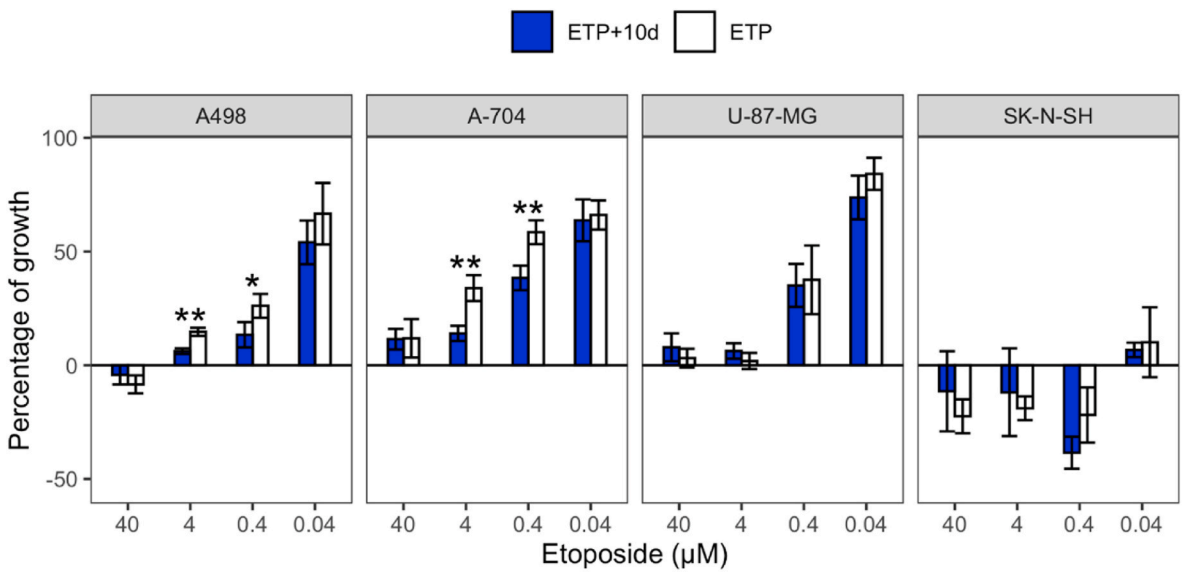

Fig. 6. Growth inhibition activity of etoposide at indicated alone and co-administered with **10d** (4 μM) in A498, A704, U87-MG, and SK-N-SH cell lines. Values are shown as mean ± SD. *p < 0.05, **p < 0.01, or ***p < 0.001.

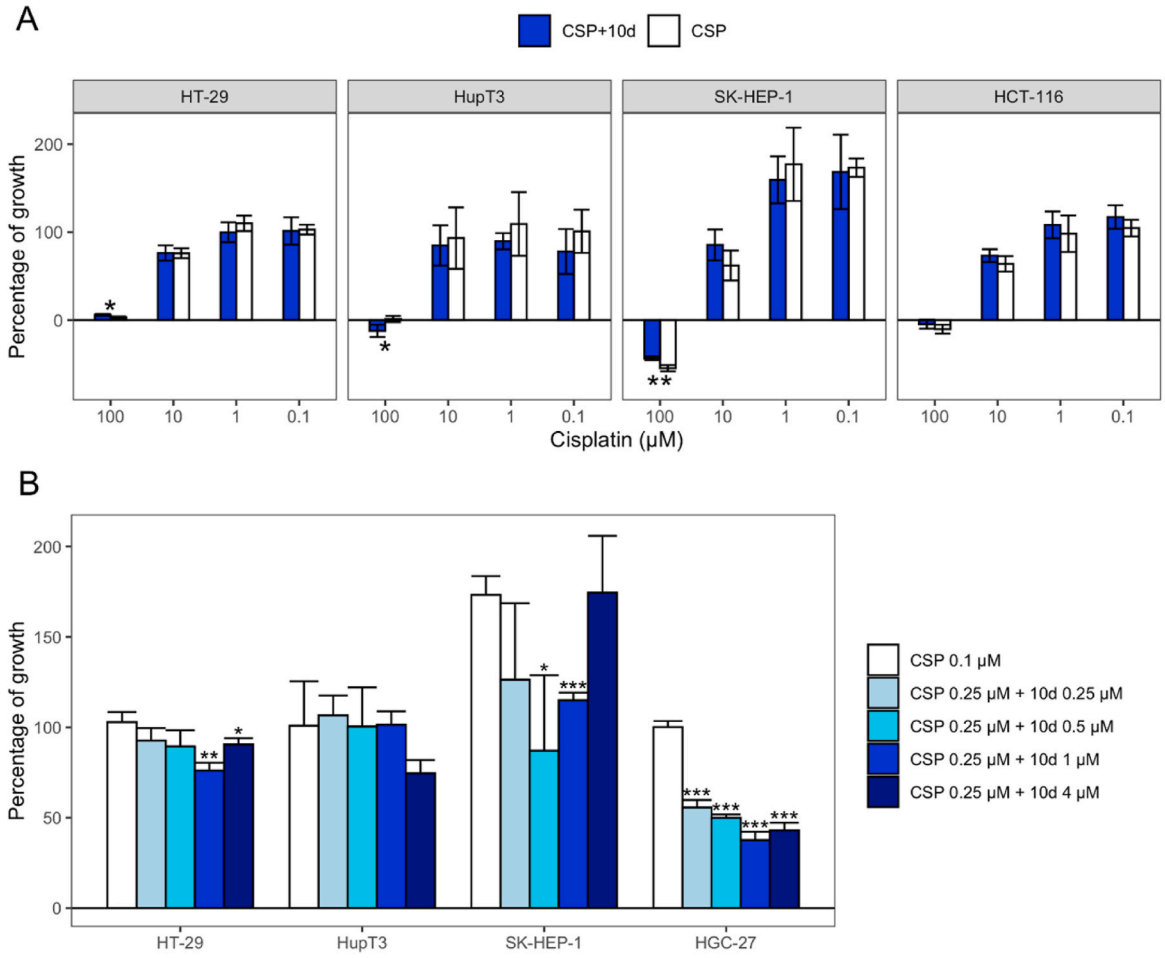

Fig. 7. A) Growth inhibition effect of **10d** (4 μM) and different combinations of cisplatin (100, 10, 1 and 0.1 μM) in HT-29, HupT3, SK-HEP1 and HCT116 cell lines; **B)** Growth inhibition effect of different combinations of **10d** (0.25, 0.5, 1 and 4 μM) and cisplatin (0.25 μM) Values are shown as mean ± SD. *p < 0.05, **p < 0.01, or ***p < 0.001.

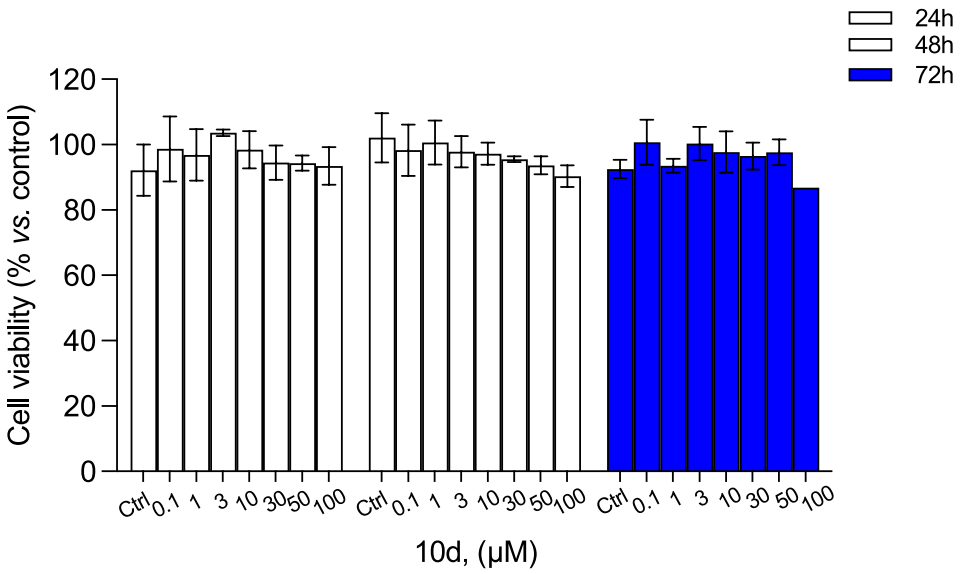

Fig. 8. MTT assay performed with increasing concentrations of **10d** at different times. Data represent means ± S.E.M. from three independent experiments, performed in triplicate (n = 3). Statistical analysis was performed by ordinary one-way ANOVA followed by Tukey's multiple comparison test.

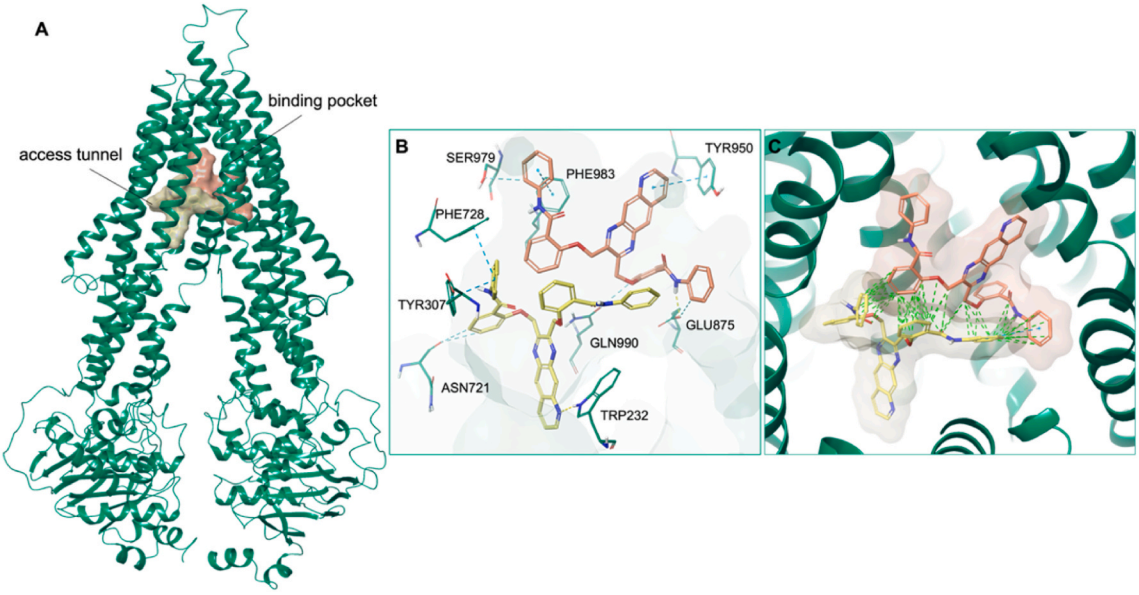

Fig. 9. 3D representation of **A)** P-gp glycoprotein binding pocket (salmon surface) and access tunnel (sand surface); **B–C)** best pose of **10d** docked into the P-gp binding pocket and into the access tunnel. The P-gp glycoprotein is represented as green cartoon, **10d** is shown as orange and yellow carbon sticks, respectively, in the binding pocket and in the access tunnel. The residues involved in crucial contacts with the compounds are reported as green carbon sticks. Hydrogen bonds, π-stacking, aromatic H-bond, and hydrophobic interactions are reported as yellow, azure, cyan and green dashed lines, respectively.

Table 2
Docking score values of compound **10d** in the investigated sites.

Compound	Docking score (kcal/mol)	
	Binding pocket	Access tunnel
10d	−13.39	−11.93

3. Discussion

Cancer drug treatment failures are mainly caused by multi-drug resistance (MDR), which is considered a major challenge in modern clinical practice. The upregulated expression of drug efflux transporter P-gp is recognized to be strongly related to MDR. Most P-gp inhibitors failed the clinical trials for adverse secondary effects. There is therefore an urgent need of new P-glycoprotein inhibitors to avoid or reduce MDR and to increase the gastrointestinal absorption of anticancer drugs. In this study, we designed and synthetized a series of nine pyridoquinoxaline-based compounds and one benzoquinoxaline derivative which were proven to interact with P-gp, restoring sensitivity to drug-resistant cancer cell lines. New P-gp inhibitors here reported were designed with small (**a-c**) or bulky (**d-i**) side chains to investigate the interactions that they could engage with one or the two binding sites in the channel of targeted efflux transporter. Compounds were predicted to be drug-like showing a good predicted ADMET profile, except for poor water solubility. Compounds were all tested at three different concentrations for the efflux pump inhibition measuring the variation in fluorescence emitted by a hydrophilic green-fluorescent dye that is trapped

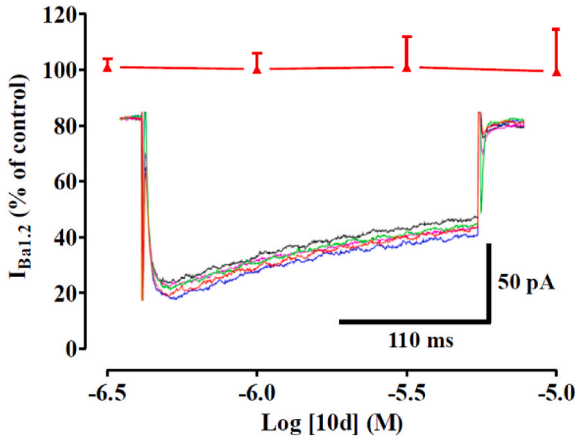

Fig. 10. Effect of **10d** on $I_{Ba1.2}$ in single rat tail artery myocytes. **10d** concentration-response curve. On the ordinate scale, the current amplitude is reported as a percentage of the control value. Data points are the mean ± SEM (n = 5). Inset: traces of $I_{Ba1.2}$ evoked by 250-ms clamp pulses to 10 mV from a V_h of −50 mV (0.067 Hz), recorded under control conditions (black) or in the presence of various concentrations of **10d** (0.3 μM red, 1 μM green, 3 μM blue, 10 μM pink, added cumulatively).

within the cell unless actively pumped out by an active ABC transporter. We observed that all the synthetized compounds actively inhibit dye efflux in most of the treated cells. Derivative **10d** was proved to be the most potent derivative by showing a significant dose-dependency in HCT-15, a cell line with a prominent P-gp/ABCB1 expression, and a superior efflux inhibition activity compared to the positive control Verapamil. Our MDR-inhibitor **10d** was also proved as the most selective derivative, being either poorly or not active in the remaining tested cell lines (overexpressing else ABC efflux pump). Derivative **10d** also revealed the best MDR reversal effect *in vitro* at poorly or non-toxic concentrations, showing increased cytotoxic activity of Vincristine both in sensitive and resistant cancer cell lines. Also, Etoposide resistance was reverted when administered together with **10d**, while cisplatin (not effluxed by P-gp) cytotoxicity was not significantly affected by the co-administration. As demonstrated for other P-gp inhibitors, the molecular modelling prediction showed that compound **10d** can recognize both the P-gp active site and the access tunnel, accommodating in a ratio of 2:1 with the target protein. In particular, **10d** was predicted to establish different kinds of interactions with the key residues of both pockets and the binding was stabilized by intermolecular interactions of the two copies of **10d**, too. Most P-gp inhibitors are endowed with off-target activities that hijack their clinical application, such as cardiotoxicity, interfering with Cav1.2 channels. Derivative **10d** was proven not to affect Cav1.2 channel function. Overall, these results suggest the use of **10d** as a novel potent MDR reversal agent for its drug efflux inhibition without undesirable toxicity in *in vivo* models.

4. Conclusions

We described a novel potent pyridoquinoxaline-based P-gp inhibitor **10d**, which showed a cancer MDR reversion effect *in vitro* assays. Starting from parental efflux inhibitors [27,28], ten quinoxaline (Qx)-based compounds were designed and synthesized and then screened for efflux inhibition of a fluorescent dye on several cancer cell lines. The most potent and selective **10d** was then assessed for MDR reversal activity when co-administered with different anticancer treatments. Vincristine and Etoposide cytotoxicity were enhanced when cells were also treated with compound **10d**. Potential binding mode, with a 2:1 ratio with P-gp, was predicted and a lack of undesired cardiotoxicity was described.

5. Material and methods

5.1. Chemistry

Nuclear magnetic resonance (^{1}H NMR and ^{13}C NMR-APT) spectra were determined in DMSO-d_6 and were recorded with a Bruker Avance III 400 NanoBay. Chemical shifts are reported in parts per million (ppm) downfield from tetramethylsilane (TMS) used as the internal standard. Splitting patterns are designated as follows: s, singlet; d, doublet; t, triplet; m, multiplet; dd, doublet of doublets. Mass spectra (MS) were performed on combined Liquid Chromatograph-Agilent 1100 series Mass Selective Detector (MSD). Melting points were carried out with a Köfler hot stage or Digital Electrothermal melting point apparatus. Analytical thin-layer chromatography (TLC) was performed on Merck silica gel F-254 plates. Pure compounds showed a single spot in TLC. For flash chromatography, Merck silica gel 60 was used with particle sizes 0.040 and 0.063 mm (230 and 400 mesh ASTM).

5.1.1. Synthesis of key intermediates 2,3-bis(bromomethyl)pyrido[2,3-g] quinoxaline (8) and 2,3-bis(bromomethyl)benzo[g]quinoxaline (12)

Quinoline-6,7-diamine (**7**), obtained as previously reported [30], or commercially available naphthalene-2,3-diamine (**11**) (1.8 mmol) was dissolved in 15 mL of hot ethanol. 1,4-dibromobutane-2,3-dione (1.2 eq) was added to the solution and the mixture was heated up to 60 °C until complete dissolution. The turning color of the solution from yellow to red, in about 15 min indicates the completing of reaction. By cooling down in ice bath the reaction mixture, the precipitation of a pure golden solid (**8** or **12**) or was achieved. Obtained yield for compound **8** of 80 %, m.p. 174–175 °C, LC/MS: *m/z* 368 ($M + H^+$); obtained yield for compound **12** of 84 %, m.p. 171–172 °C, LC/MS: *m/z* 367 ($M + H^+$).

5.1.2. Synthesis of compounds 10a-i and 13d

2,3-bis(bromomethyl)pyrido[2,3-g]quinoxaline (**8**) (0.95 mmol) and the appropriate substituted phenols (**9a-i**) (1.9 mmol) were dissolved in 15 mL of chloroform. To this, an aqueous solution (15 mL) of sodium hydroxide (1.9 mmol) and benzyltriethylammonium chloride – BTAC (1.9 mmol) was added. The mixture was heated at 60 °C for 27h (**10b**, **c**), 48h (**10a**, **d**, **e**), 72h (**10f**, **h**), 7 days (**10g**, **i**). At the end, the two phases were separated. The organic phase was washed with water, dried off and evaporated obtaining an oil that when grinded with diethyl ether gained a pink, beige or brown solid. Compound **13d** was obtained through the same procedure but starting from previously synthetized compound **12**, final derivative **13d** was obtained after 12h, and after work up a yellow solid was gained.

5.2. Experimental section - characterisation of final derivatives 10a-i and 13d

5.2.1. 4,4'-(pyrido[2,3-g]quinoxaline-2,3-diylbis(methylene))bis(oxy) dibenzonitrile (10a)

Compound **10a** was obtain with 45 % yield; mp: 178–180 °C; TLC (diethyl ether/ethanol, 8/2) R_f: 0.79; IR (nujol): 1740, 1604 cm^{-1}. ^{1}H NMR (400 MHz, DMSO-d_6) δ 9.13 (d, J = 3.4 Hz, 1H, H-7), 8.84 (s, 1H, H-5), 8.74 (s, 1H, H-10), 8.70 (d, J = 8.7 Hz, 1H, H-9), 7.79 (dd, J = 8.3, 4.0 Hz, 4H, H-3′,5′,3″,5″), 7.72–7.64 (m, 1H, H-8), 7.27 (t, J = 8.4 Hz, 4H, H-2′,6′,2″,6″), 5.76 (d, J = 5.1 Hz, 4H, 2xCH_2). ^{13}C NMR (101 MHz, DMSO-d_6) δ 161.98, 161.93, 154.02, 151.99, 151.85, 146.60, 139.28, 137.32, 137.16, 134.68, 134.59, 129.44, 128.76, 128.08, 122.82, 119.97, 119.46, 116.85, 116.44, 116.41, 103.93, 101.39, 69.50, 69.28. LC/MS for $C_{27}H_{17}N_5O_2$ (MW: 443.47) *m/z*: 444 $[M+H]^+$. Elemental analysis: calculated for $C_{27}H_{17}N_5O_2$ C 73.13, H 3.86, N 15.79; measured C 73.24, H 3.88, N 15.69.

5.2.2. Dimethyl-4,4'-(pyrido[2,3-g]quinoxaline-2,3-diylbis(methylene))bis (oxy)bis(3-methoxybenzoate) (10b)

Compound **10b** was obtain with 45 % yield; mp: 180–182 °C; TLC

(diethyl ether/ethanol 8/2) R_f: 0.75; IR (nujol): 1712, 1599 cm^{-1}. ^1H NMR (400 MHz, DMSO-d_6) δ 9.15 (d, J = 2.4 Hz, 1H, H-7), 8.88 (s, 1H, H-10), 8.78 (s, 1H, H-5), 8.72 (d, J = 8.5 Hz, 1H, H-9), 7.69 (dd, J = 8.6, 3.9 Hz, 1H, H-8), 7.52 (dt, J = 18.8, 6.2 Hz, 2H, 2xH-5′), 7.34 (d, J = 1.7 Hz, 2H, 2xH-3′), 7.22 (dd, J = 13.1, 8.5 Hz, 2H, 2xH-6′), 5.76 (d, J = 5.2 Hz, 4H, 2xCH_2), 3.81 (d, J = 5.3 Hz, 6H, 2xCOO$\underline{CH_3}$), 3.77 (d, J = 1.3 Hz, 4H, 2x OCH_3). ^{13}C NMR (101 MHz, DMSO-d_6) δ 165.78, 153.57, 151.91, 151.78, 148.47, 146.22, 138.81, 136.86, 136.70, 129.04, 122.66, 122.61, 122.57, 122.37, 113.01, 112.92, 111.69, 70.40, 70.15, 55.46, 51.89. LC/MS m/z 570 $[M+H]^+$. Elemental analysis: calculated for $C_{31}H_{27}N_3O_8$ C 65.37, H 4.78, N 7.38; measured C 65.34, H 4.88, N 7.27.

5.2.3. Dimethyl-2,2'-(pyrido[2,3-g]quinoxaline-2,3-diylbis(methylene))bis (oxy)dibenzoate (10c)

Compound **10c** was obtain with 50 % yield; mp: 142–144 °C; TLC (diethyl ether/acetone 9/1) R_f: 0.62; IR (nujol): 1705, 1584 cm^{-1}. ^1H NMR (400 MHz, DMSO-d_6) δ 9.10 (d, J = 3.5 Hz, 1H, H-7), 8.76 (s, 1H, H-10), 8.67 (d, J = 8.5 Hz, 1H, H-9), 8.63 (s, 1H, H-5), 7.85 (t, J = 7.5 Hz, 2H, 2xH-5′), 7.77 (dd, J = 25.8, 8.1 Hz, 2H, H-3′), 7.64 (m, 1H, H-8), 7.56 (dd, J = 8.7, 8.1 Hz, 2H, 2xH-6′), 7.28 (t, J = 7.3 Hz, 2H, 2xH-4′), 4.87 (s, 4H, 2xCH_2), 3.81 (d, J = 5.4 Hz, 6H, 2xOCH_3). ^{13}C NMR (101 MHz, DMSO-d_6) δ 166.21, 153.15, 152.97, 152.73, 145.95, 139.24, 138.86, 138.73, 136.77, 136.58, 132.53, 132.51, 130.49, 130.44, 128.58, 128.49, 128.21, 128.12, 127.80, 127.62, 126.98, 125.10, 124.94, 122.05, 52.13, 36.62, 36.53. LC/MS m/z 542 $[M+H]^+$. Elemental analysis: calculated for $C_{29}H_{23}N_3O_4S_2$ C 64.31, H 4.28, N 7.76, S 11.84; measured C 64.39, H 4.35, N 7.77, S 11.79.

5.2.4. 2,2'-(pyrido[2,3-g]quinoxaline-2,3-diylbis(methylene))bis(oxy)bis (N-phenylbenzamide) (10d)

Compound **10d** was obtained with 93 % yield; mp: 213–215 °C; TLC (ether) R_f: 0.48; IR (nujol): 1648, 1597, 1539, cm^{-1}. ^1H NMR (400 MHz, DMSO-d_6) δ 10.81 (s, 1H, NH), 10.76 (s, 1H, NH), 9.10 (d, J = 3.6 Hz, 1H, H-7), 8.59 (s, 1H, H-10), 8.53 (s, 1H, H-5), 8.50 (d, J = 8.7 Hz, 1H, H-9), 7.86 (t, J = 6.8 Hz, 2H, 2xH-5′), 7.71 (dd, J = 14.5, 7.9 Hz, 4H, 2xH-2″,6″), 7.64 (dd, J = 8.5, 3.9 Hz, 1H, H-8), 7.58–7.44 (m, 4H, 2xH-3″,5″), 7.29 (td, J = 7.7, 4.5 Hz, 4H, 2xH-4′,6′), 7.13 (dt, J = 21.6, 7.3 Hz, 4H, 2xH-3′,4″), 5.96 (s, 4H, 2xCH_2). ^{13}C NMR (101 MHz, DMSO-d_6) δ 163.92, 155.35, 155.30, 153.51, 152.15, 151.88, 146.06, 138.79, 138.75, 138.67, 136.71, 136.41, 132.44, 132.37, 130.47, 130.39, 128.69, 128.63, 127.91, 127.48, 124.39, 124.33, 123.93, 123.89, 122.39, 121.52, 121.46, 120.65, 120.37, 113.62, 113.60, 68.63. LC/MS m/z 632 $[M+H]^+$. Elemental analysis: calculated for $C_{39}H_{29}N_5O_4$ C 74.15, H 4.63, N 11.09; measured C 74.29, H 4.45, N 11.12.

5.2.5. 2,2'-(pyrido[2,3-g]quinoxaline-2,3-diylbis(methylene))bis(oxy)bis (N-(4-methoxyphenyl)benzamide) (10e)

Compound **10e** was obtain with 25 % yield; mp: 127–130 °C; TLC (diethyl ether/acetone 9/1) R_f: 0.31; IR (nujol): 1646, 1599, 1537 cm^{-1}; ^1H NMR (400 MHz, DMSO-d_6) δ 10.74 (s, 1H, NH), 10.69 (s, 1H, NH), 9.10 (d, J = 2.0 Hz, 1H, H-7), 8.53 (s, 1H, H-5), 8.46 (m, 2H, H-9,10), 7.88 (t, J = 6.8 Hz, 2H, 2xH-5′), 7.80–7.35 (m, 9H, H-8, 2xH-3′,4′, 2xH-2″,6″), 7.16 (ws, 2H, 2xH-6′), 6.86 (dd, J = 7.0, 6.3 Hz, 4H, 2xH-3″,5″), 5.94 (s, 4H, 2xCH_2), 3.73 (s, 6H, 2xCH_3). ^{13}C NMR (101 MHz, DMSO-d_6) δ 164.04, 163.94, 156.33, 156.23, 155.84, 155.78, 153.94, 152.56, 152.27, 146.49, 139.12, 137.16, 136.76, 134.12, 132.86, 132.80, 132.28, 132.23, 130.98, 130.91, 129.04, 128.32, 127.99, 124.70, 124.62, 123.31, 123.03, 122.69, 122.00, 119.38, 117.72, 114.32, 114.28, 114.09, 69.05, 55.60. LC/MS m/z 692 $[M+H]^+$. Elemental analysis: calculated for $C_{41}H_{33}N_5O_6$ C 71.19, H 4.81, N 10.12; measured C 71.27, H 4.75, N 10.09.

5.2.6. 6,6'-(pyrido[2,3-g]quinoxaline-2,3-diylbis(methylene))bis(oxy)bis (3-chloro-N-(4-methoxyphenyl) benzamide) (10f)

Compound **10f** was obtain with 25 % yield; mp: 230–231 °C; TLC (ether/ethanol 8/2) R_f: 0.23; IR (nujol): 1640, 1599 cm^{-1}. ^1H NMR (400 MHz, DMSO-d_6) δ: 10.69 (s, 1H, NH), 10.65 (s, 1H, NH), 9.10 (s, 1H, H-7), 8.50 (m, 3H), 7.89–7.36 (m, 10H), 6.92 (m, 5H), 5.92 (s, 4H, CH_2), 3.75 (d, 6H, 2xOCH_3). ^{13}C NMR (DMSO-d_6) δ: solubility is too low that was not possible to record any readable data. LC/MS m/z 761 $[M+H]^+$. Elemental analysis: calculated for $C_{41}H_{31}Cl_2N_5O_6$ C 64.74, H 4.11, Cl 9.32, N 9.21; measured C 64.79, H 4.22, Cl 9.33, N 9.18.

5.2.7. 6,6'-(pyrido[2,3-g]quinoxaline-2,3-diylbis(methylene))bis(oxy)bis (3-chloro-N-(3,5-dimethoxyphenyl) benzamide) (10g)

Compound **10g** was obtain with 30 % yield; mp: >300 °C; TLC (ether/ethanol 8/2) R_f: 0.22; IR (nujol): 1640, 1600 cm^{-1}. ^1H NMR (400 MHz, DMSO-d_6) δ 10.65 (s, 1H, NH), 10.62 (s, 1H, NH), 9.11 (s, 1H, H-7), 8.61 (d, J = 8 Hz, 2H, H-5,10), 8.53 (d, J = 8 Hz, 1H, H-9), 7.77 (d, J = 8 Hz, 2H, 2xH-5′), 7.67 (m, 1H, H-8), 7.52 (s, 4H, 2xH-3′,6′), 6.88 (s, 4H, 2xH-2″,6″), 6.26 (d, J = 8 Hz, 2H, 2xH-4″), 5.91 (s, 4H, 2xCH_2), 3.57 (s, 12H, 4xOCH_3). ^{13}C NMR (101 MHz, DMSO-d_6) δ 164.85, 160.44, 156.53, 140.36, 140.21, 140.01, 139.67, 138.44, 132.96, 128.37, 125.29, 122.75, 122.40, 122.36, 120.98, 119.86, 119.01, 108.74, 98.93, 96.25, 69.30, 55.17. LC/MS m/z 821, 823 $[M+H]^+$. Elemental analysis: calculated for $C_{43}H_{35}Cl_2N_5O_8$ C 62.93, H 4.30, Cl 8.64, N 8.53; measured C 62.99, H 4.27, Cl 8.63, N 8.48.

5.2.8. 6,6'-(pyrido[2,3-g]quinoxaline-2,3-diylbis(methylene))bis(oxy)bis (3-chloro-N-(3,4,5-trimethoxyphenyl) benzamide) (10h)

Compound **10h** was obtain with 90 % yield; mp: 121–123 °C; TLC (ether/acetone 9/1) R_f: 0.17; IR (nujol): 1640, 1589 cm^{-1}. ^1H NMR (400 MHz, DMSO-d_6) δ 10.68 (s, 1H, NH),10.64 (s, 1H, NH), 9.06 (d, J = 2.1 Hz, 1H, H-7), 8.53 (d, J = 6.9 Hz, 1H, H-10), 8.47 (d, J = 8.5 Hz, 1H, H-9), 8.31 (s, 1H, H-5), 7.79 (s, 2H, 2xH-3′), 7.63 (m, 1H, H-8), 7.52 (s, 4H, H-5′,6′), 6.98 (s, 4H, 2xH-2″,6″), 5.92 (s, 4H, 2xCH_2), 3.64 (s, 6H, 2x*p*-OCH_3), 3.50 (s, 12H, 4x*m*-OCH_3). ^{13}C NMR (101 MHz, DMSO-d_6) δ 162.52, 154.09, 152.66, 151.78, 151.55, 146.00, 138.58, 136.64, 136.21, 134.47, 131.64, 129.54, 128.63, 127.92, 127.68, 126.28, 125.33, 122.40, 115.68, 98.67, 98.59, 69.26, 69.15, 60.07, 55.46. LC/MS m/z 881, 883 $[M+H]^+$. Elemental analysis: calculated for $C_{45}H_{39}Cl_2N_5O_{10}$ C 61.37, H 4.46, Cl 8.05, N 7.95; measured C 61.47, H 4.52, Cl 8.08, N 7.99.

5.2.9. 6,6'-(pyrido[2,3-g]quinoxaline-2,3-diylbis(methylene))bis(oxy)bis (3-chloro-N-(3,4-dichlorophenyl) benzamide) (10i)

Compound **10i** was obtain with 42 % yield; mp: 216–217 °C; TLC (ether/ethanol 8/2) R_f: 0.21; IR (nujol): 1638, 1590 cm^{-1}. ^1H NMR (400 MHz, DMSO-d_6) δ 10.90 (s, 1H, NH), 10.85 (s, 1H, NH), 9.10 (d, J = 3.8 Hz, 1H, H-7), 8.58 (m, 3H, H-5,9,10), 7.96 (m, 1H, H-8), 7.80 (d, J = 7.4 Hz, 2H, 2x-H3'), 7.71–7.56 (m, 4H, 2xH-5′,2″), 7.56–7.37 (m, 6H, 2xH-4′,5″,6″), 7.15 (m, 2H, 2xH-6′), 5.92 (s, 4H, 2xCH_2). ^{13}C NMR (101 MHz, DMSO-d_6) δ 166.57, 164.46, 161.04, 155.32, 153.61, 153.22, 152.03, 151.84, 150.15, 146.10, 145.66, 138.86, 138.80, 137.33, 136.48, 134.96, 133.52, 132.59, 130.90, 130.61, 129.28, 128.82, 128.58, 127.53, 127.10, 125.23, 124.18, 123.18, 122.37, 121.63, 120.48, 118.92, 117.98, 117.60, 117.54, 116.67, 113.68, 87.30, 68.82. LC/MS m/z 770, 772 $[M+H]^+$. Elemental analysis: calculated for $C_{39}H_{25}Cl_4N_5O_4$ C 60.88, H 3.27, Cl 18.43, N 9.10; measured C 60.95, H 4.22, Cl 18.49, N 9.20.

5.2.10. 2,2'-((benzo[g]quinoxaline-2,3-diylbis(methylene))bis(oxy))bis (N-phenylbenzamide) (13d)

Compound **13d** was obtained with 68 % yield; m.p. 224–225 °C; TLC (petroleum ether/ethyl acetate) R_f: 0.42. ^1H NMR (400 MHz, DMSO-d_6) δ 10.81 (s, 2H, 2xNH), 8.45 (s, 2H, H-5,10), 8.05 (dd, J = 6.4, 3.2 Hz, 2H, H-6,9), 7.87 (d, J = 7.4 Hz, 2H, 2xH-3′), 7.70 (d, J = 7.7 Hz, 4H, 2xH-5″,6″), 7.65 (dd, J = 6.5, 3.1 Hz, 2H, H-7,8), 7.50 (d, J = 3.6 Hz, 4H, 2xH-5′,6′), 7.31 (t, J = 7.8 Hz, 4H, 2xH-3″,5″), 7.22–7.06 (m, 4H, 2xH-4′, 2xH-4″), 5.93 (s, 4H, 2xCH_2). ^{13}C NMR (101 MHz, DMSO-d_6) δ 163.94, 155.39, 151.15, 138.79, 136.65, 133.24, 132.40, 130.43, 128.68,

128.15, 127.33, 126.91, 124.28, 123.97, 121.43, 120.81, 113.56, 68.60, 40.13, 39.92, 39.71, 39.50, 39.29, 39.08, 38.87. LC/MS *m/z* 631 $[M+H]^+$. Elemental analysis: calculated for $C_{40}H_{30}N_4O_4$ C 76.17, H 4.79, N 8.88; measured C 76.29, H 4.74, N 8.76.

5.3. Computational studies

5.3.1. Library preparation

The compounds' library was prepared by means of LigPrep tool (Schrödinger Release 2018-1: LigPrep, Schrödinger, LLC, New York, NY, 2018), hydrogens were added, salts were removed, ionization states were calculated using Ionizer at pH 7.0 ± 2.0 and then each structure was submitted to MacroModel energy minimization using OPLS_2005 as force field (Schrödinger Release 2018-1: MacroModel, Schrödinger, LLC, New York, NY, 2018).

5.3.2. ADME prediction

The energy-minimized ligands' structures were evaluated for their drug-like properties, by means of the Qikprop module v. 5.5 (Schrödinger Release 2018-1: QikProp, Schrödinger, LLC, New York, NY, 2018). In detail, QikProp predicts physically significant descriptors of organic molecules and provides ranges for comparing a particular molecule's properties with those of 95 % of known drugs.

5.3.3. Docking studies

Starting from the Encequidar-bound human P-glycoprotein in complex with UIC2-Fab, deposited in the Protein Data Bank (PDB) with the PDB code 7O9W [37], our molecular recognition studies were carried out.

The receptor structure was prepared by means of the Protein Preparation Wizard tool implemented in Maestro, using OLPS_2005 as force field. Residual crystallographic buffer components and UIC2 fab-fragment chains were removed, missing side chains were built, hydrogen atoms were added, side chains protonation states at pH 7.0 ± 2.0 were assigned (Schrödinger Release 2018-1: Protein Preparation Wizard, Schrödinger, LLC, New York, NY, 2018).

In order to evaluate the reliability of our molecular recognition approach, we performed redocking calculations by using Glide Extra Precision (XP) protocol, (Schrödinger Release 2018-1: Glide, Schrödinger, LLC, New York, NY, 2018) [38], that was able to reproduce the experimentally determined binding mode, in fact, we obtained a Root Mean Square Deviation (RMSD) value equal to 1.57 Å.

The docking studies were performed by means of Glide v7.8 XP algorithm (Schrödinger Release 2018-1: Glide, Schrödinger, LLC, New York, NY, 2018, [38]), and 10 poses were generated.

5.4. Biological evaluation

5.4.1. Cell culture

A498, A-704, U-87-MG, Mewo, HT-29, Hup-T3, HGC-27, SK-HEP-1, SK-N-SH were obtained from IRCCS University Hospital San Martino—IST National Institute for Cancer Research (Genova, Italy). HCT-116 were obtained from Dr. Jun Yokota, Cancer Genome Group, Institute of Predictive and Personalized Medicine of Cancer (Barcelona, Spain). A498, A-704, HCT-116, HGC-27, HT-29, Hup-T3, Mewo, PC-3, SK-HEP-1, U-87-MG were cultured in DMEM high glucose (Euroclone ECM0101L) supplemented with 10 % FBS, 2 mM L-Glutamine (Sigma G7513), non-essential amino acids (Sigma M7145), Sodium Piruvate 1 mM (Sigma S8636), and Antibiotic Antimycotic Solution (Sigma A5955). SK-N-SH were cultured in RPMI1640 (Euroclone ECB9006L) supplemented with 10 % FBS (Euroclone ECS0180L), 2 mM L-Glutamine (Sigma G7513) and Antibiotic Antimycotic Solution (Sigma A5955).

5.4.2. MDR assay

EFLUXX-ID Green multidrug resistance assay kit was performed to assess relative activity of MDR efflux pumps in culture cells in presence or absence of ABC inhibitors. 24 h before compound addition, 5000 cells suspended in 20 μL phenol-red free complete medium were plated in each well of a 384 Well Flat Clear Bottom Black Polystyrene TC-Treated Microplate (Corning 3764). The day after, 5 μL of compounds were added to each sample to obtain indicated treatment concentrations. Plating of cells, preparation of serial dilutions and addition of compounds to cells were performed using an automated liquid handling platform (Gilson Pipetmax). After 15 min of treatment, EFLUXX-ID Green Detection Reagent at 1:200 concentration and 1 μg/mL Hoechst-33342 were added to each sample. Samples were incubated for additional 30 min at 37 °C, 5 % CO_2 humidified air before analysis. Images for blue fluorescence and green fluorescence detection were taken with objective 4x using the automated digital widefield microscopy system BioTek Cytation 5. Cell's area in each image were delimited as the area external to blue-fluorescent nucleus with a radius of 5 μM and green fluorescence signal intensity (GFI) in each area was quantified. 250 events were randomly selected from each image and median GFI was calculated. Then, median GFI of each sample was normalized to median GFI of untreated samples from 3 wells (median GFI from 250 events, divided by median GFI of untreated samples from 750 events). Mean value and standard deviation of three normalized median values from three technical replicates (three images from three distinct wells) was calculated. One-tailed student's t-test was performed to assess increased normalized median GFI in treated samples compared to normalized median GFI in untreated ones.

5.4.3. Cell proliferation assays

500 cells suspended in 20 μL containing SiR-DNA (Tebu-bio SC007) and CellTox Green Dye (Promega G8731) were plated in each well of a 384 Well Flat Clear Bottom Black Polystyrene TC-Treated Microplates (Corning 3764). The day after, 10 μL of serial dilutions of compounds in complete medium without phenol red were added to each sample. Immediately after compound addition to cells and after 72 h from treatment, images for far-red fluorescence, green fluorescence and phase contrast were taken with objective 4x using automated digital widefield microscopy system BioTek Cytation 5. For each well, 4 images were taken and merged to cover the entire well. Number of nuclei, stained by SiR-DNA in far-red fluorescence, and number of dead cells, stained by CellTox Green Dye in green fluorescence, were automatically counted using BioTek Gen5 software. Live cells were calculated by subtracting number of dead cells from total count of nuclei and percentage of growth was calculated as previously reported [39,40]. Three technical replicates were performed. Two-tailed student's t-tests were performed to assess differences between treatments as indicated in figures.

5.5. Cytotoxicity

5.5.1. Cell cultures

Human microglial clone 3 cell line (HMC3) (ATCC® CRL-3304™) was cultured in in high glucose DMEM (Corning, Tewksbury, MA, USA) supplemented with 10 % FBS, streptomycin (100 g/mL) and penicillin (100 U/mL) (Sigma-Aldrich, Milan, Italy) at 37 °C, 5 % CO_2 humidified air.

5.5.2. MTT (cell viability assay)

The 3-(4,5-dimethylthiazol-2- yl)-2,5-diphenyltetrazolium bromide (MTT) reagent was used to test the effects of **10d** on cell viability. Briefly, after the pertinent treatment, cells were incubated with MTT (0.5 mg/mL) for 4 h at 37 °C. The formazan products were dissolved in DMSO and absorbance at OD540 nm was determined with an automated microplate reader (BIO-TEK, Winooski, VT, United States). The percentage of cell viability was calculated as the percentage of control cells.

5.5.3. Statistical analysis

Obtained results are expressed as the mean ± standard error of the mean (S.E.M.). Statistical analyses were performed using commercial

software (GraphPad Prism, San Diego, CA, USA) using ordinary one-way ANOVA followed by Tukey's post hoc test. Differences for which $p < 0.05$ were considered significant.

5.6. Off target evaluation: Cav1.2 channel blockade

5.6.1. Animal care statement

The Animal Care and Ethics Committee of the University of Siena and the Italian Department of Health (7DF19.N.TBT) approved all the procedures, in strict accordance with the European Union Guidelines for the Care and the Use of Laboratory Animals (European Union Directive 2010/63/EU). An isoflurane (4 %) and O_2 gas mixture was used to anaesthetize male Wistar rats (250–350 g; Charles River Italia, Calco, Italy) with Fluovac (Harvard Apparatus, Holliston, Massachusetts, USA), before decapitation and exsanguination. The tail main artery was immersed in external solution and processed as detailed below.

5.6.2. Cell isolation method

Smooth muscle cells were dissociated from an 8-mm long piece of the tail main artery incubated at 37 °C for 35–45 min in 2 mL of external solution (see below for composition) containing 0.1 mM Ca^{2+}, 20 mM taurine (equally balanced with NaCl), 1.1 mg/mL collagenase (type XI), 1 mg/mL soybean trypsin inhibitor, and 1 mg/mL BSA, bubbled with carboxygen (95 % O_2–5% CO_2) [41]. External solution (in mM): 130 NaCl, 5.6 KCl, 10 HEPES, 20 glucose, 1.2 $MgCl_2$, and 5 Na-pyruvate; pH 7.4. The cell suspension, stored in 0.05 mM Ca^{2+}, 20 mM taurine, and 0.5 mg/mL BSA external solution at 4 °C, was used for a maximum of two days [42].

5.6.3. Whole-cell patch-clamp recordings

The junction potential, whole-cell capacitance, and series resistance (between 70 % and 75 %) were compensated with an Axopatch 200B patch-clamp amplifier (Molecular Devices Corporation, Sunnyvale, CA, USA) in conjunction with an ADC/DAC interface (DigiData 1200 A/B series, Molecular Devices Corporation), which applied voltage pulses to, and recorded membrane currents from myocytes. Borosilicate glass recording electrodes (WPI, Berlin, Germany) had a pipette resistance of 2–4 MΩ. Low-pass filtered (1 kHz) current signals, recorded under the conventional whole-cell configuration at 20–22 °C, were digitized at 3 kHz [43].

5.6.4. Ba^{2+} currents through $Ca_V1.2$ channel ($I_{Ba1.2}$) recordings

A peristaltic pump (LKB 2132, Bromma, Sweden) superfused (flow rate of 400 μl/min) cells with a 0.1 mM Ca^{2+} and 30 mM tetraethylammonium (TEA) external solution. The internal solution contained (in mM) 100 CsCl, 10 HEPES, 11 EGTA, 2 $MgCl_2$, 1 $CaCl_2$ (free Ca^{2+} concentration pCa 8.4), 5 Na pyruvate, 5 succinic acid, 5 oxaloacetic acid, 3 Na_2ATP, and 5 phosphocreatine (pH 7.4 with CsOH). $I_{Ba1.2}$ [44] elicited with 250-ms clamp pulses (0.067 Hz) to 10 mV from a V_h of −50 mV and recorded in 30 mM TEA and 5 mM Ba^{2+} external solution, stabilized in 7–10 min after the whole-cell configuration had been obtained, and did not run down during the following 40 min [45]. TEA and Cs^+, in the external and internal solution, respectively, blocked K^+ currents, whereas 10 μM nifedipine, completely blocking $I_{Ba1.2}$, allowed leakage and residual outward currents measurement offline. The external solution containing 30 mM TEA- and 5 mM Ba^{2+}, and the internal solution had an osmolarity of 320 mosmol and 290 mosmol, respectively (as measured by an Osmostat OM 6020 osmometer, Menarini Diagnostics, Florence, Italy).

5.6.5. Materials

The chemicals used were: BSA, collagenase (type XI), nifedipine, taurine, TEA chloride, and soybean trypsin inhibitor (Sigma Chimica, Milan, Italy). Nifedipine was dissolved directly in ethanol, **10d** in DMSO. Neither DMSO nor ethanol (maximal concentration of 0.1 %, v/v) affected vascular responses (data not shown).

Funding

This work was funded by MUR (Ministero dell'Università e della Ricerca) through "Fondo per il Programma Nazionale di Ricerca e Progetti di Rilevante Interesse Nazionale (PRIN)" with the project code "PRINCARTA2020" and "PON AIM - Attraction and International Mobility" program.

CRediT authorship contribution statement

Roberta Ibba: Writing – review & editing, Writing – original draft, Investigation, Formal analysis, Data curation, Conceptualization. **Simona Sestito:** Writing – review & editing, Writing – original draft, Formal analysis. **Francesca Alessandra Ambrosio:** Writing – review & editing, Investigation. **Emanuela Marchese:** Writing – review & editing, Investigation. **Giosuè Costa:** Writing – review & editing, Formal analysis, Data curation. **Francesco Paolo Fiorentino:** Writing – review & editing, Investigation. **Fabio Fusi:** Writing – review & editing, Investigation, Formal analysis. **Irene Marchesi:** Writing – review & editing, Investigation. **Beatrice Polini:** Writing – review & editing, Investigation. **Grazia Chiellini:** Writing – review & editing, Data curation. **Stefano Alcaro:** Writing – review & editing, Data curation. **Sandra Piras:** Writing – review & editing, Supervision, Resources, Funding acquisition, Formal analysis, Data curation, Conceptualization. **Antonio Carta:** Writing – review & editing, Supervision, Resources, Funding acquisition, Conceptualization.

Declaration of competing interest

The authors declare the following financial interests/personal relationships which may be considered as potential competing interests: Antonio Carta reports financial support was provided by Ministry of Education and Merit. Simona Sestito reports financial support was provided by Ministry of Education and Merit. If there are other authors, they declare that they have no known competing financial interests or personal relationships that could have appeared to influence the work reported in this paper.

Data availability

No data was used for the research described in the article.

Acknowledgments

We would like to thank MUR (Ministero dell'Università e della Ricerca) which funded this research through the above-mentioned programs and the fellowship to SS within the "PON AIM - Attraction and International Mobility" program.

Appendix A. Supplementary data

Supplementary data to this article can be found online at https://doi.org/10.1016/j.ejmech.2024.116647.

References

[1] J. Goebel, J. Chmielewski, C.A. Hrycyna, The roles of the human ATP-binding cassette transporters P-glycoprotein and ABCG2 in multidrug resistance in cancer and at endogenous sites: future opportunities for structure-based drug design of inhibitors, Cancer Drug Resistance 4 (2021), https://doi.org/10.20517/cdr.2021.19.

[2] O.C. Demurtas, R. Francisco, G. Diretto, P. Ferrante, S. Frusciante, M. Pietrella, G. Aprea, L. Borghi, M. Feeney, L. Frigerio, A. Coricello, G. Costa, S. Alcaro, E. Martinoia, G. Giuliano, ABCC transporters mediate the vacuolar accumulation of crocins in saffron stigmas, Plant Cell (2019) 00193, https://doi.org/10.1105/tpc.19.00193 (2019) tpc.

[3] A.T. Fojo, K. Ueda, D.J. Slamon, D.G. Poplack, M.M. Gottesman, I. Pastan, Expression of a multidrug-resistance gene in human tumors and tissues, Proc. Natl. Acad. Sci. USA 84 (1987) 265–269, https://doi.org/10.1073/pnas.84.1.265.

[4] Q. Wu, Z. Yang, Y. Nie, Y. Shi, D. Fan, Multi-drug resistance in cancer chemotherapeutics: mechanisms and lab approaches, Cancer Lett. 347 (2014) 159–166, https://doi.org/10.1016/j.canlet.2014.03.013.

[5] K. Beis, Structural basis for the mechanism of ABC transporters, Biochem. Soc. Trans. 43 (2015) 889–893, https://doi.org/10.1042/BST20150047.

[6] K.O. Alfarouk, C.-M. Stock, S. Taylor, M. Walsh, A.K. Muddathir, D. Verduzco, A.H. H. Bashir, O.Y. Mohammed, G.O. Elhassan, S. Harguindey, S.J. Reshkin, M. E. Ibrahim, C. Rauch, Resistance to cancer chemotherapy: failure in drug response from ADME to P-gp, Cancer Cell Int. 15 (2015) 71, https://doi.org/10.1186/s12935-015-0221-1.

[7] P. Labrie, S.P. Maddaford, S. Fortin, S. Rakhit, L.P. Kotra, R.C. Gaudreault, A comparative molecular field analysis (CoMFA) and comparative molecular similarity indices analysis (CoMSIA) of anthranilamide derivatives that are multidrug resistance modulators, J. Med. Chem. 49 (2006) 7646–7660, https://doi.org/10.1021/jm060239b.

[8] J.I. Fletcher, R.T. Williams, M.J. Henderson, M.D. Norris, M. Haber, ABC transporters as mediators of drug resistance and contributors to cancer cell biology, Drug Resist. Updates 26 (2016) 1–9, https://doi.org/10.1016/j.drup.2016.03.001.

[9] A.M. Kurimchak, C. Herrera-Montávez, S. Montserrat-Sangrà, D. Araiza-Olivera, J. Hu, R. Neumann-Domer, M. Kuruvilla, A. Bellacosa, J.R. Testa, J. Jin, J. S. Duncan, The drug efflux pump MDR1 promotes intrinsic and acquired resistance to PROTACs in cancer cells, Sci. Signal. 15 (2022), https://doi.org/10.1126/scisignal.abn2707.

[10] R. Milroy, A randomised clinical study of verapamil in addition to combination chemotherapy in small cell lung cancer, Br. J. Cancer 68 (1993) 813–818, https://doi.org/10.1038/bjc.1993.433.

[11] L. Saltz, B. Murphy, N. Kemeny, J. Bertino, W. Tong, D. Keefe, Y. Tzy-Jun, Y. Tao, D. Kelsen, J.P. O'Brien, A phase I trial of intrahepatic Verapamil and doxorubicin. Regional therapy to overcome multidrug resistance, Cancer 74 (1994) 2757–2764, https://doi.org/10.1002/1097-0142(19941115)74:10<2757::AID-CNCR2820741004>3.0.CO;2-O.

[12] N.L. Bartlett, B.L. Lum, G.A. Fisher, N.A. Brophy, M.N. Ehsan, J. Halsey, B.I. Sikic, Phase I trial of doxorubicin with cyclosporine as a modulator of multidrug resistance, J. Clin. Oncol. 12 (1994) 835–842, https://doi.org/10.1200/JCO.1994.12.4.835.

[13] A.F. List, C. Spier, J. Greer, S. Wolff, J. Hutter, R. Dorr, S. Salmon, B. Futscher, M. Baier, W. Dalton, Phase I/II trial of cyclosporine as a chemotherapy-resistance modifier in acute leukemia, J. Clin. Oncol. 11 (1993) 1652–1660, https://doi.org/10.1200/JCO.1993.11.9.1652.

[14] R. Jones, D. Kerr, A. Harnett, E. Rankin, S. Ray, S. Kaye, A pilot study of quinidine and epirubicin in the treatment of advanced breast cancer, Br. J. Cancer 62 (1990) 133–135, https://doi.org/10.1038/bjc.1990.244.

[15] R.J. Motzer, P. Lyn, P. Fischer, P. Lianes, R.L. Ngo, C. Cordon-Cardo, J.P. O'Brien, Phase I/II trial of dexverapamil plus vinblastine for patients with advanced renal cell carcinoma, J. Clin. Oncol. 13 (1995) 1958–1965, https://doi.org/10.1200/JCO.1995.13.8.1958.

[16] C. Punt, E. Voest, E. Tueni, A. Van Oosterom, A. Backx, P. De Mulder, B. Hecquet, C. Lucas, B. Gerard, H. Bleiberg, Phase IB study of doxorubicin in combination with the multidrug resistance reversing agent S9788 in advanced colorectal and renal cell cancer, Br. J. Cancer 76 (1997) 1376–1381, https://doi.org/10.1038/bjc.1997.563.

[17] R. Stupp, J. Bauer, O. Pagani, B. Gerard, T. Cerny, C. Sessa, G. Bastian, M. Sarkany, J. Schläpfer, B. Giroux, S. Leyvraz, Ventricular arrhythmia and torsade de pointe: Dose limiting toxicities of the MDR-modulator S9788 in a phase I trial, Ann. Oncol. 9 (1998) 1233–1242, https://doi.org/10.1023/A:1008495919071.

[18] S. Yuan, B. Wang, Q.-Q. Dai, X.-N. Zhang, J.-Y. Zhang, J.-H. Zuo, H. Liu, Z.-S. Chen, G.-B. Li, S. Wang, H.-M. Liu, B. Yu, Discovery of new 4-indolyl quinazoline derivatives as highly potent and orally bioavailable P-glycoprotein inhibitors, J. Med. Chem. 64 (2021) 14895–14911, https://doi.org/10.1021/acs.jmedchem.1c01452.

[19] Y. Kono, I. Kawahara, K. Shinozaki, I. Nomura, H. Marutani, A. Yamamoto, T. Fujita, Characterization of P-glycoprotein inhibitors for evaluating the effect of P-glycoprotein on the intestinal absorption of drugs, Pharmaceutics 13 (2021) 388, https://doi.org/10.3390/pharmaceutics13030388.

[20] J.-I. Lai, Y.-J. Tseng, M.-H. Chen, C.-Y.F. Huang, P.M.-H. Chang, Clinical perspective of FDA approved drugs with P-glycoprotein inhibition activities for potential cancer therapeutics, Front. Oncol. 10 (2020), https://doi.org/10.3389/fonc.2020.561936.

[21] A. Kumar, V. Jaitak, Natural products as multidrug resistance modulators in cancer, Eur. J. Med. Chem. 176 (2019) 268–291, https://doi.org/10.1016/j.ejmech.2019.05.027.

[22] G. Yalcin-Ozkat, Molecular modeling strategies of cancer multidrug resistance, Drug Resist. Updates 59 (2021) 100789, https://doi.org/10.1016/J.DRUP.2021.100789.

[23] X. Quan, H. Du, J. Xu, X. Hou, X. Gong, Y. Wu, Y. Zhou, J. Jiang, L. Lu, S. Yuan, X. Yang, L. Shi, L. Sun, Novel quinoline compound derivatives of NSC23925 as potent reversal agents against P-Glycoprotein-Mediated multidrug resistance, Front. Chem. 7 (2019), https://doi.org/10.3389/fchem.2019.00820.

[24] S. Wang, S.-Q. Wang, Q.-X. Teng, L. Yang, Z.-N. Lei, X.-H. Yuan, J.-F. Huo, X.-B. Chen, M. Wang, B. Yu, Z.-S. Chen, H.-M. Liu, Structure-based design, synthesis, and biological evaluation of new triazolo[1,5- α]pyrimidine derivatives as highly potent and orally active ABCB1 modulators, J. Med. Chem. 63 (2020) 15979–15996, https://doi.org/10.1021/acs.jmedchem.0c01741.

[25] C.D. Smith, C.B. Myers, J.T. Zilfou, S.N. Smith, D.S. Lawrence, Indoloquinoxaline compounds that selectively antagonize P-glycoprotein, Oncol. Res. 12 (2001) 219–229, https://doi.org/10.3727/096504001108747710.

[26] A. Di Pietro, L.D. Chiaradia-Delatorre, C. Gauthier, A. Mascarello, R.A. Yunes, R. J. Nunes, T.B. Crecynski-Pasa, P.C. Leal, E. Winter, G. Gozzi, N. Daflon-Yunes, R. Terreux, S. Cadena, Quinoxaline-substituted chalcones as new inhibitors of breast cancer resistance protein ABCG2: polyspecificity at B-ring position, Drug Des. Dev. Ther. 609 (2014), https://doi.org/10.2147/DDDT.S56625.

[27] A. Carta, M. Loriga, S. Piras, G. Paglietti, P. La Colla, B. Busonera, G. Collu, R. Loddo, Synthesis of variously substituted 3-Phenoxymethyl Quinoxalin-2-ones and quinoxalines capable to potentiate in vitro the antiproliferative activity of anticancer drugs in multi-drug resistant cell lines, Med. Chem. 2 (2006) 113–122, https://doi.org/10.2174/157340606776056197.

[28] A. Carta, S. Piras, G. Paglietti, S. Pricl, P. Colla, B. Busonera, R. Loddo, 2(3)-Arylthio(oxy)-methylquinoxaline derivatives: a new class of P-Glycoprotein-Mediated drug efflux inhibitors, Med. Chem. 4 (2008) 194–205, https://doi.org/10.2174/157340608784325197.

[29] A.S. Tikhomirov, V.B. Tsvetkov, Y.L. Volodina, V.A. Litvinova, D.V. Andreeva, L. G. Dezhenkova, D.N. Kaluzhny, I.D. Treshalin, A.A. Shtil, A.E. Shchekotikhin, Heterocyclic ring expansion yields anthraquinone derivatives potent against multidrug resistant tumor cells, Bioorg. Chem. 127 (2022) 105925, https://doi.org/10.1016/j.bioorg.2022.105925.

[30] P. Sanna, A. Carta, G. Paglietti, Synthesis of two novel tricyclic rings: Triazolo[4,5-g]quinolines and pyrido[2,3-g]quinoxalines derived from 6,7-diaminoquinolines, Heterocycles 53 (2000) 423, https://doi.org/10.3987/COM-99-8766.

[31] J. Barretina, G. Caponigro, N. Stransky, K. Venkatesan, A.A. Margolin, S. Kim, C. J. Wilson, J. Lehár, G.V. Kryukov, D. Sonkin, A. Reddy, M. Liu, L. Murray, M. F. Berger, J.E. Monahan, P. Morais, J. Meltzer, A. Korejwa, J. Jané-Valbuena, F. A. Mapa, J. Thibault, E. Bric-Furlong, P. Raman, A. Shipway, I.H. Engels, J. Cheng, G.K. Yu, J. Yu, P. Aspesi, M. de Silva, K. Jagtap, M.D. Jones, L. Wang, C. Hatton, E. Palescandolo, S. Gupta, S. Mahan, C. Sougnez, R.C. Onofrio, T. Liefeld, L. MacConaill, W. Winckler, M. Reich, N. Li, J.P. Mesirov, S.B. Gabriel, G. Getz, K. Ardlie, V. Chan, V.E. Myer, B.L. Weber, J. Porter, M. Warmuth, P. Finan, J. L. Harris, M. Meyerson, T.R. Golub, M.P. Morrissey, W.R. Sellers, R. Schlegel, L. A. Garraway, The Cancer Cell Line Encyclopedia enables predictive modelling of anticancer drug sensitivity, Nature 483 (2012) 603–607, https://doi.org/10.1038/nature11003.

[32] R. Maia, P-glycoprotein and survivin simultaneously regulate vincristine-induced apoptosis in chronic myeloid leukemia cells, Int. J. Oncol. (2011), https://doi.org/10.3892/ijo.2011.1103.

[33] K. Robinson, V. Tiriveedhi, Perplexing role of P-glycoprotein in tumor microenvironment, Front. Oncol. 10 (2020), https://doi.org/10.3389/fonc.2020.00265.

[34] J.S. Lagas, L. Fan, E. Wagenaar, M.L.H. Vlaming, O. van Tellingen, J.H. Beijnen, A. H. Schinkel, P-Glycoprotein (P-gp/Abcb1), Abcc2, and Abcc3 determine the pharmacokinetics of etoposide, Clin. Cancer Res. 16 (2010) 130–140, https://doi.org/10.1158/1078-0432.CCR-09-1321.

[35] T. Kobori, S. Harada, K. Nakamoto, S. Tokuyama, Mechanisms of P-glycoprotein alteration during anticancer treatment: role in the pharmacokinetic and pharmacological effects of various substrate drugs, J. Pharmacol. Sci. 125 (2014) 242–254, https://doi.org/10.1254/jphs.14R01CR.

[36] A. Tamaki, C. Ierano, G. Szakacs, R.W. Robey, S.E. Bates, The controversial role of ABC transporters in clinical oncology, Essays Biochem. 50 (2011) 209–232, https://doi.org/10.1042/BSE0500209.

[37] S. Urgaonkar, K. Nosol, A.M. Said, N.N. Nasief, Y. Bu, K.P. Locher, J.Y.N. Lau, M. P. Smolinski, Discovery and characterization of potent dual P-glycoprotein and CYP3A4 inhibitors: design, synthesis, cryo-EM analysis, and biological evaluations, J. Med. Chem. 65 (2022) 191–216, https://doi.org/10.1021/acs.jmedchem.1c01272.

[38] R.A. Friesner, R.B. Murphy, M.P. Repasky, L.L. Frye, J.R. Greenwood, T.A. Halgren, P.C. Sanschagrin, D.T. Mainz, Extra precision Glide: docking and scoring incorporating a model of hydrophobic enclosure for Protein−Ligand complexes, J. Med. Chem. 49 (2006) 6177–6196, https://doi.org/10.1021/jm051256o.

[39] M.R. Boyd, K.D. Paull, L.R. Rubinstein, Data display and analysis strategies for the NCI disease-oriented in vitro antitumor drug screen, in: Cytotoxic Anticancer Drugs: Models and Concepts for Drug Discovery and Development, Springer US, Boston, MA, 1992, pp. 11–34, https://doi.org/10.1007/978-1-4615-3492-1_2.

[40] F.P. Fiorentino, L. Bagella, I. Marchesi, A new parameter of growth inhibition for cell proliferation assays, J. Cell. Physiol. 233 (2018) 4106–4115, https://doi.org/10.1002/jcp.26208.

[41] A. Trezza, O. Spiga, P. Mugnai, S. Saponara, G. Sgaragli, F. Fusi, Functional, electrophysiology, and molecular dynamics analysis of quercetin-induced contraction of rat vascular musculature, Eur. J. Pharmacol. 918 (2022) 174778, https://doi.org/10.1016/j.ejphar.2022.174778.

[42] G. Carullo, A. Ahmed, A. Trezza, O. Spiga, A. Brizzi, S. Saponara, F. Fusi, F. Aiello, A multitarget semi-synthetic derivative of the flavonoid morin with improved in vitro vasorelaxant activity: role of CaV1.2 and KCa1.1 channels, Biochem. Pharmacol. 185 (2021) 114429, https://doi.org/10.1016/j.bcp.2021.114429.

[43] F. Fusi, A. Trezza, G. Sgaragli, O. Spiga, S. Saponara, S. Bova, Ritanserin blocks CaV1.2 channels in rat artery smooth muscles: electrophysiological, functional, and computational studies, Acta Pharmacol. Sin. 41 (2020) 1158–1166, https://doi.org/10.1038/s41401-020-0370-1.

[44] N.M. Cuong, N.T. Son, N.T. Nhan, P.N. Khanh, T.T. Huong, N.T.T. Tram, G. Sgaragli, A. Ahmed, A. Trezza, O. Spiga, F. Fusi, Vasorelaxing activity of R-(−)-3′-Hydroxy-2,4,5-trimethoxydalbergiquinol from Dalbergia tonkinensis: involvement of smooth muscle CaV1.2 channels, Planta Med. 86 (2020) 284–293, https://doi.org/10.1055/a-1099-2929.

[45] F. Fusi, A. Trezza, O. Spiga, G. Sgaragli, S. Bova, Ca v 1.2 channel current block by the PKA inhibitor H-89 in rat tail artery myocytes via a PKA-independent

mechanism: electrophysiological, functional, and molecular docking studies, Biochem. Pharmacol. 140 (2017) 53–63, https://doi.org/10.1016/j.bcp.2017.05.020.